EUROPEAN ORGANIZATION FOR NUCLEAR RESEARCH

CERN-EP-2003-031
26 May 2003

Tests of models of color reconnection and a search for glueballs using gluon jets with a rapidity gap

The OPAL Collaboration

Abstract

Gluon jets with a mean energy of 22 GeV and purity of 95% are selected from hadronic Z^0 decay events produced in e^+e^- annihilations. A subsample of these jets is identified which exhibits a large gap in the rapidity distribution of particles within the jet. After imposing the requirement of a rapidity gap, the gluon jet purity is 86%. These jets are observed to demonstrate a high degree of sensitivity to the presence of color reconnection, i.e. higher order QCD processes affecting the underlying color structure. We use our data to test three QCD models which include a simulation of color reconnection: one in the Ariadne Monte Carlo, one in the Herwig Monte Carlo, and the other by Rathsman in the Pythia Monte Carlo. We find the Rathsman and Ariadne color reconnection models can describe our gluon jet measurements only if very large values are used for the cutoff parameters which serve to terminate the parton showers, and that the description of inclusive Z^0 data is significantly degraded in this case. We conclude that color reconnection as implemented by these two models is disfavored. The signal from the Herwig color reconnection model is less clear and we do not obtain a definite conclusion concerning this model. In a separate study, we follow recent theoretical suggestions and search for glueball-like objects in the leading part of the gluon jets. No clear evidence is observed for these objects.

(Submitted to Eur. Phys. J. C)

The OPAL Collaboration

G. Abbiendi[2], C. Ainsley[5], P.F. Åkesson[3], G. Alexander[22], J. Allison[16], P. Amaral[9], G. Anagnostou[1], K.J. Anderson[9], S. Arcelli[2], S. Asai[23], D. Axen[27], G. Azuelos[18,a], I. Bailey[26], E. Barberio[8,p], R.J. Barlow[16], R.J. Batley[5], P. Bechtle[25], T. Behnke[25], K.W. Bell[20], P.J. Bell[1], G. Bella[22], A. Bellerive[6], G. Benelli[4], S. Bethke[32], O. Biebel[31], O. Boeriu[10], P. Bock[11], M. Boutemeur[31], S. Braibant[8], L. Brigliadori[2], R.M. Brown[20], K. Buesser[25], H.J. Burckhart[8], S. Campana[4], R.K. Carnegie[6], B. Caron[28], A.A. Carter[13], J.R. Carter[5], C.Y. Chang[17], D.G. Charlton[1], A. Csilling[29], M. Cuffiani[2], S. Dado[21], A. De Roeck[8], E.A. De Wolf[8,s], K. Desch[25], B. Dienes[30], M. Donkers[6], J. Dubbert[31], E. Duchovni[24], G. Duckeck[31], I.P. Duerdoth[16], E. Etzion[22], F. Fabbri[2], L. Feld[10], P. Ferrari[8], F. Fiedler[31], I. Fleck[10], M. Ford[5], A. Frey[8], A. Fürtjes[8], P. Gagnon[12], J.W. Gary[4], G. Gaycken[25], C. Geich-Gimbel[3], G. Giacomelli[2], P. Giacomelli[2], M. Giunta[4], J. Goldberg[21], E. Gross[24], J. Grunhaus[22], M. Gruwé[8], P.O. Günther[3], A. Gupta[9], C. Hajdu[29], M. Hamann[25], G.G. Hanson[4], K. Harder[25], A. Harel[21], M. Harin-Dirac[4], M. Hauschild[8], C.M. Hawkes[1], R. Hawkings[8], R.J. Hemingway[6], C. Hensel[25], G. Herten[10], R.D. Heuer[25], J.C. Hill[5], K. Hoffman[9], D. Horváth[29,c], P. Igo-Kemenes[11], K. Ishii[23], H. Jeremie[18], P. Jovanovic[1], T.R. Junk[6], N. Kanaya[26], J. Kanzaki[23,u], G. Karapetian[18], D. Karlen[26], K. Kawagoe[23], T. Kawamoto[23], R.K. Keeler[26], R.G. Kellogg[17], B.W. Kennedy[20], D.H. Kim[19], K. Klein[11,t], A. Klier[24], S. Kluth[32], T. Kobayashi[23], M. Kobel[3], S. Komamiya[23], L. Kormos[26], T. Krämer[25], P. Krieger[6,l], J. von Krogh[11], K. Kruger[8], T. Kuhl[25], M. Kupper[24], G.D. Lafferty[16], H. Landsman[21], D. Lanske[14], J.G. Layter[4], A. Leins[31], D. Lellouch[24], J. Letts[o], L. Levinson[24], J. Lillich[10], S.L. Lloyd[13], F.K. Loebinger[16], J. Lu[27,w], J. Ludwig[10], A. Macpherson[28,i], W. Mader[3], S. Marcellini[2], A.J. Martin[13], G. Masetti[2], T. Mashimo[23], P. Mättig[m], W.J. McDonald[28], J. McKenna[27], T.J. McMahon[1], R.A. McPherson[26], F. Meijers[8], W. Menges[25], F.S. Merritt[9], H. Mes[6,a], A. Michelini[2], S. Mihara[23], G. Mikenberg[24], D.J. Miller[15], S. Moed[21], W. Mohr[10], T. Mori[23], A. Mutter[10], K. Nagai[13], I. Nakamura[23,V], H. Nanjo[23], H.A. Neal[33], R. Nisius[32], S.W. O'Neale[1], A. Oh[8], A. Okpara[11], M.J. Oreglia[9], S. Orito[23,*], C. Pahl[32], G. Pásztor[4,g], J.R. Pater[16], G.N. Patrick[20], J.E. Pilcher[9], J. Pinfold[28], D.E. Plane[8], B. Poli[2], J. Polok[8], O. Pooth[14], M. Przybycień[8,n], A. Quadt[3], K. Rabbertz[8,r], C. Rembser[8], P. Renkel[24], J.M. Roney[26], S. Rosati[3], Y. Rozen[21], K. Runge[10], K. Sachs[6], T. Saeki[23], E.K.G. Sarkisyan[8,j], A.D. Schaile[31], O. Schaile[31], P. Scharff-Hansen[8], J. Schieck[32], T. Schörner-Sadenius[8], M. Schröder[8], M. Schumacher[3], C. Schwick[8], W.G. Scott[20], R. Seuster[14,f], T.G. Shears[8,h], B.C. Shen[4], P. Sherwood[15], G. Siroli[2], A. Skuja[17], A.M. Smith[8], R. Sobie[26], S. Söldner-Rembold[16,d], F. Spano[9], A. Stahl[3], K. Stephens[16], D. Strom[19], R. Ströhmer[31], S. Tarem[21], M. Tasevsky[8], R.J. Taylor[15], R. Teuscher[9], M.A. Thomson[5], E. Torrence[19], D. Toya[23], P. Tran[4], I. Trigger[8], Z. Trócsányi[30,e], E. Tsur[22], M.F. Turner-Watson[1], I. Ueda[23], B. Ujvári[30,e], C.F. Vollmer[31], P. Vannerem[10], R. Vértesi[30], M. Verzocchi[17], H. Voss[8,q], J. Vossebeld[8,h], D. Waller[6], C.P. Ward[5], D.R. Ward[5], P.M. Watkins[1], A.T. Watson[1], N.K. Watson[1], P.S. Wells[8], T. Wengler[8], N. Wermes[3], D. Wetterling[11] G.W. Wilson[16,k], J.A. Wilson[1], G. Wolf[24], T.R. Wyatt[16], S. Yamashita[23], D. Zer-Zion[4], L. Zivkovic[24]

[1]School of Physics and Astronomy, University of Birmingham, Birmingham B15 2TT, UK
[2]Dipartimento di Fisica dell' Università di Bologna and INFN, I-40126 Bologna, Italy

[3]Physikalisches Institut, Universität Bonn, D-53115 Bonn, Germany
[4]Department of Physics, University of California, Riverside CA 92521, USA
[5]Cavendish Laboratory, Cambridge CB3 0HE, UK
[6]Ottawa-Carleton Institute for Physics, Department of Physics, Carleton University, Ottawa, Ontario K1S 5B6, Canada
[8]CERN, European Organisation for Nuclear Research, CH-1211 Geneva 23, Switzerland
[9]Enrico Fermi Institute and Department of Physics, University of Chicago, Chicago IL 60637, USA
[10]Fakultät für Physik, Albert-Ludwigs-Universität Freiburg, D-79104 Freiburg, Germany
[11]Physikalisches Institut, Universität Heidelberg, D-69120 Heidelberg, Germany
[12]Indiana University, Department of Physics, Bloomington IN 47405, USA
[13]Queen Mary and Westfield College, University of London, London E1 4NS, UK
[14]Technische Hochschule Aachen, III Physikalisches Institut, Sommerfeldstrasse 26-28, D-52056 Aachen, Germany
[15]University College London, London WC1E 6BT, UK
[16]Department of Physics, Schuster Laboratory, The University, Manchester M13 9PL, UK
[17]Department of Physics, University of Maryland, College Park, MD 20742, USA
[18]Laboratoire de Physique Nucléaire, Université de Montréal, Montréal, Québec H3C 3J7, Canada
[19]University of Oregon, Department of Physics, Eugene OR 97403, USA
[20]CLRC Rutherford Appleton Laboratory, Chilton, Didcot, Oxfordshire OX11 0QX, UK
[21]Department of Physics, Technion-Israel Institute of Technology, Haifa 32000, Israel
[22]Department of Physics and Astronomy, Tel Aviv University, Tel Aviv 69978, Israel
[23]International Centre for Elementary Particle Physics and Department of Physics, University of Tokyo, Tokyo 113-0033, and Kobe University, Kobe 657-8501, Japan
[24]Particle Physics Department, Weizmann Institute of Science, Rehovot 76100, Israel
[25]Universität Hamburg/DESY, Institut für Experimentalphysik, Notkestrasse 85, D-22607 Hamburg, Germany
[26]University of Victoria, Department of Physics, P O Box 3055, Victoria BC V8W 3P6, Canada
[27]University of British Columbia, Department of Physics, Vancouver BC V6T 1Z1, Canada
[28]University of Alberta, Department of Physics, Edmonton AB T6G 2J1, Canada
[29]Research Institute for Particle and Nuclear Physics, H-1525 Budapest, P O Box 49, Hungary
[30]Institute of Nuclear Research, H-4001 Debrecen, P O Box 51, Hungary
[31]Ludwig-Maximilians-Universität München, Sektion Physik, Am Coulombwall 1, D-85748 Garching, Germany
[32]Max-Planck-Institute für Physik, Föhringer Ring 6, D-80805 München, Germany
[33]Yale University, Department of Physics, New Haven, CT 06520, USA

[a] and at TRIUMF, Vancouver, Canada V6T 2A3
[c] and Institute of Nuclear Research, Debrecen, Hungary
[d] and Heisenberg Fellow
[e] and Department of Experimental Physics, Lajos Kossuth University, Debrecen, Hungary
[f] and MPI München
[g] and Research Institute for Particle and Nuclear Physics, Budapest, Hungary
[h] now at University of Liverpool, Dept of Physics, Liverpool L69 3BX, U.K.
[i] and CERN, EP Div, 1211 Geneva 23
[j] and Manchester University

[k] now at University of Kansas, Dept of Physics and Astronomy, Lawrence, KS 66045, U.S.A.
[l] now at University of Toronto, Dept of Physics, Toronto, Canada
[m] current address Bergische Universität, Wuppertal, Germany
[n] now at University of Mining and Metallurgy, Cracow, Poland
[o] now at University of California, San Diego, U.S.A.
[p] now at Physics Dept Southern Methodist University, Dallas, TX 75275, U.S.A.
[q] now at IPHE Université de Lausanne, CH-1015 Lausanne, Switzerland
[r] now at IEKP Universität Karlsruhe, Germany
[s] now at Universitaire Instelling Antwerpen, Physics Department, B-2610 Antwerpen, Belgium
[t] now at RWTH Aachen, Germany
[u] and High Energy Accelerator Research Organisation (KEK), Tsukuba, Ibaraki, Japan
[v] now at University of Pennsylvania, Philadelphia, Pennsylvania, USA
[w] now at TRIUMF, Vancouver, Canada
[*] Deceased

1 Introduction

Rapidity y, defined by $y = \frac{1}{2}\ln\left(\frac{E+p_\parallel}{E-p_\parallel}\right)$ with E the energy of a particle and $p_\parallel$ the component of its 3-momentum along an axis[1], is one of the most common variables used to characterize the phase space distribution of particles in high energy collisions. Of current interest (see for example [2]) are events with a so-called rapidity gap, namely events in which two populated regions in rapidity are separated by an interval devoid of particles. High energy collisions are often characterized by the formation of quark and gluon jets, i.e. collimated streams of hadrons associated with the hard scattering of quarks and gluons, respectively. Most recent interest in rapidity gaps has focused on a class of events in electron-proton [3] and proton-antiproton [4] collisions with large rapidity gaps between jets: these events are interpreted as arising from the exchange of a strongly interacting color singlet object, such as a pomeron [5], between the underlying partonic constituents of the event.

Another source of rapidity gaps is color reconnection (CR), i.e. a rearrangement of the underlying color structure of an event from its simplest configuration, in which a color flux tube or "string" is stretched from a quark to an antiquark through intermediate gluons in a manner such that string segments do not cross (a so-called planar diagram, see Fig. 1a), to a more complex pattern in which some segments can either cross or else appear as disconnected entities whose endpoints are gluons (Fig. 1b). Diagrams with color reconnection represent higher order processes in Quantum Chromodynamics (QCD), suppressed by order $1/N_{\rm C}^2$ compared to planar diagrams, where $N_{\rm C} = 3$ is the number of colors. In models of hadron production such as the Lund string model [6], the flux tubes hadronize. In events with a disconnected gluonic string segment as in Fig. 1b, a rapidity gap can form between the isolated segment – often the leading (highest rapidity) part of a gluon jet – and the rest of the event. Thus rapidity gaps in gluon jets can provide a sensitive means to search for effects of color reconnection. Color reconnection has been a topic of considerable recent interest because of its potential effects in fully hadronic decays of $\mathrm{W^+W^-}$ events produced in electron-positron ($\mathrm{e^+e^-}$) collisions [7], introducing an uncertainty in the measurement of the W boson mass at LEP [8].

Recently [9], gluon jets with a rapidity gap were also proposed as a potentially favorable environment for the production of color singlet bound states of gluons, such as glueballs, through diagrams like Fig.1b in which the isolated gluonic system represents a hadronic resonance.

Previous studies of rapidity gaps in $\mathrm{e^+e^-}$ hadronic annihilations were based on inclusive $\mathrm{Z^0}$ events and separated two- and three-jet events from $\mathrm{Z^0}$ decays [10]. The rapidity distribution of charged particles in gluon jets was used to test models of color reconnection in [11]. There are no previously published experimental studies on gluon jets with a rapidity gap.

In this paper, we study gluon jets with rapidity gaps, produced in three-jet quark-antiquark-gluon ($\mathrm{q\overline{q}g}$) events from $\mathrm{e^+e^-}$ hadronic $\mathrm{Z^0}$ decays. The gluon jets are identified through "anti-tagging," using displaced secondary vertices from B hadrons to identify the quark and anti-quark jets. The data were collected with the OPAL detector at the LEP $\mathrm{e^+e^-}$ storage ring at CERN. We measure the charged particle multiplicity, total electric charge, and distributions of invariant mass in the leading part of the gluon jets.

[1] Usually the thrust [1], jet, or beam axis.

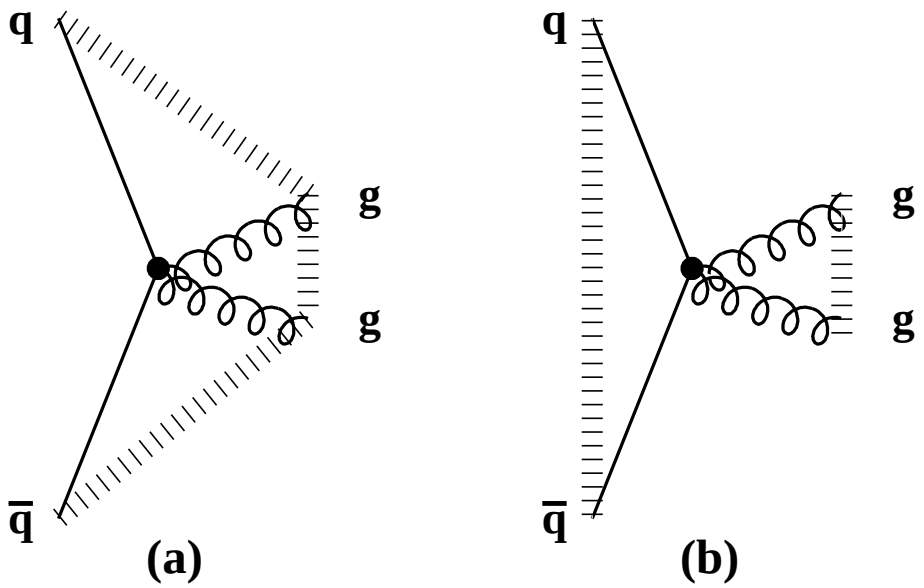

Figure 1: Schematic illustrations of events with (a) standard "planar" color flow and (b) reconnection. The hatched regions represent color flux tubes or "strings" stretched between the quark q, antiquark $\overline{\mathrm{q}}$ and gluons g.

2 Detector and data sample

The OPAL detector is described in detail elsewhere [12, 13]. OPAL operated from 1989 to 2000 and subsequently was dismantled. The tracking system consisted of a silicon microvertex detector, an inner vertex chamber, a large volume jet chamber, and specialized chambers at the outer radius of the jet chamber to improve the measurements in the z-direction.[2] The tracking system covered the region $|\cos\theta| < 0.98$ and was enclosed by a solenoidal magnet coil with an axial field of 0.435 T. Electromagnetic energy was measured by a lead-glass calorimeter located outside the magnet coil, which also covered $|\cos\theta| < 0.98$.

The present analysis is based on a sample of about 2 722 000 hadronic annihilation events, corresponding to the OPAL sample collected within 3 GeV of the Z^0 peak from 1993 to 1995. This sample includes readout of both the r-ϕ and z coordinates of the silicon strip microvertex detector [13]. The procedures for identifying hadronic annihilation events are described in [14].

We employ the tracks of charged particles reconstructed in the tracking chambers and clusters of energy deposited in the electromagnetic calorimeter. Charged tracks are required to have at least 20 measured points (of 159 possible) in the jet chamber, or at least 50% of the number of points expected based on the track's polar angle, whichever is larger. In addition, the tracks are required to have a momentum component perpendicular to the beam axis greater than 0.05 GeV/c, to lie in the region $|\cos\theta| < 0.96$, to point to the origin to within 5 cm in the r-ϕ plane and 30 cm in the z direction, and to yield a reasonable χ^2 per degree-of-freedom for

[2]Our right handed coordinate system is defined so that z is parallel to the e^- beam axis, x points towards the center of the LEP ring, r is the coordinate normal to the beam axis, ϕ is the azimuthal angle around the beam axis with respect to x, and θ is the polar angle with respect to z.

the track fit in the r-ϕ plane. Electromagnetic clusters are required to have an energy greater than 0.10 GeV if they are in the barrel section of the detector ($|\cos\theta| < 0.82$) or 0.25 GeV if they are in the endcap section ($0.82 < |\cos\theta| < 0.98$). A matching algorithm [15] is employed to reduce double counting of energy in cases where charged tracks point towards electromagnetic clusters. Specifically, if a charged track points towards a cluster, the cluster's energy is redefined by subtracting the energy which is expected to be deposited in the calorimeter by the track. If the energy of the cluster is smaller than this expected energy, the cluster is not used. In this way, the energies of the clusters are primarily associated with neutral particles.

Each accepted track and cluster is considered to be a particle. Tracks are assigned the pion mass. Clusters are assigned zero mass since they originate mostly from photons.

To eliminate residual background and events in which a significant number of particles is lost near the beam direction, the number of accepted charged tracks in an event is required to be at least five and the thrust axis of the event, calculated using the particles, is required to satisfy $|\cos(\theta_{\rm thrust})| < 0.90$, where $\theta_{\rm thrust}$ is the angle between the thrust and beam axes. The number of events which passes these cuts is 2 407 000. The residual background to this sample from all sources is estimated to be less than 1% [14] and is neglected.

3 QCD models

To establish the sensitivity of our analysis to processes with color reconnection, we generate events using Monte Carlo simulations of perturbative QCD and the hadronization process, both with and without the effects of reconnection.

The models without reconnection in our study are the Jetset [16], Herwig [17, 18] and Ariadne [19] Monte Carlo programs, versions 7.4, 6.2 and 4.11 respectively. Jetset and Herwig are based on parton showers with branchings described by Altarelli-Parisi splitting functions [20], followed by string hadronization [6] for Jetset and cluster hadronization [21] for Herwig. Ariadne employs the dipole cascade model [22] to generate a parton shower, followed by string hadronization. The principal parameters of the models were tuned to yield an optimized description of the global properties of hadronic Z^0 events and are documented in [23] for Jetset and in Tables 1 and 2 for Herwig and Ariadne. All three models provide a good description of the main features of e^+e^- hadronic annihilation events, including the properties of identified gluon jets, see for example [11].

The models in our study which incorporate color reconnection are the model of Lönnblad [25] implemented in the Ariadne Monte Carlo[3], the color reconnection model [18] in the Herwig Monte Carlo, and a model introduced by Rathsman [27]. We refer to these as the Ariadne-CR, Herwig-CR, and Rathsman-CR models, respectively. The Ariadne-CR model is an extension of the model of Gustafson and Häkkinen [28]. The Rathsman-CR model is implemented in the Pythia Monte Carlo [16], version 5.7. For e^+e^- annihilations in the absence of initial-state

[3]There are three variants of the color reconnection model in Ariadne, corresponding to settings of the parameter MSTA(35)=1, 2 or 3; for hard processes involving a single color singlet system, such as Z^0 decays, all three variants are identical; note that the parameter PARA(28) should be set to zero if the MSTA(35)=2 option is used in Z^0 decays [26].

Parameter	Monte Carlo name	Default value	Optimized value
$\Lambda_{\rm QCD}$ (GeV)	QCDLAM	0.18	0.18 ± 0.01
Gluon mass (GeV/c^2)	RMASS(13)	0.75	0.75 ± 0.05
Maximum cluster mass parameter (GeV/c^2)	CLMAX	3.35	3.35 ± 0.05
Maximum cluster mass parameter	CLPOW	2.00	2.0 ± 0.2
Cluster spectrum parameter, udsc	PSPLT(1)	1.00	1.00 ± 0.05
Cluster spectrum parameter, b	PSPLT(2)	1.00	$0.33^{+0.07}_{-0.03}$
Gaussian smearing parameter, udsc	CLSMR(1)	0.0	$0.40^{+0.20}_{-0.02}$
Decuplet baryon weight	DECWT	1.0	0.7 ± 0.1

Table 1: OPAL parameter set for Herwig, version 6.2. The method used to tune the parameters is presented in [23]. Parameters not listed were left at their default values. The uncertainties represent ± 1 standard deviation limits obtained from the χ^2 contours. The χ^2 contours were defined by varying the parameters one at a time from their tuned values.

Parameter	Monte Carlo name	Default value	Optimized value
$\Lambda_{\rm QCD}$ (GeV)	PARA(1)	0.22	0.215 ± 0.002
$p_{T,\rm min.}$ (GeV/c)	PARA(3)	0.60	0.70 ± 0.05
b (GeV^{-2})	PARJ(42)	0.58	0.63 ± 0.01
$\mathcal{P}(qq)/\mathcal{P}(q)$	PARJ(1)	0.10	0.130 ± 0.003
$[\mathcal{P}(us)/\mathcal{P}(ud)]$ / $[\mathcal{P}(s)/\mathcal{P}(d)]$	PARJ(3)	0.40	0.600 ± 0.016
$\mathcal{P}(ud_1)/3\mathcal{P}(ud_0)$	PARJ(4)	0.05	$0.040^{+0.010}_{-0.003}$
Extra Baryon suppression (MSTJ(12) = 3)	PARJ(19)	1.00	0.52

Table 2: OPAL parameter set for Ariadne, version 4.11. The method used to tune the parameters is presented in [23]. Parameters not listed were left at their default values. The extra baryon suppression factor PARJ(19), enabled by setting MSTJ(12) = 3, was taken from [24]. The uncertainties have the same meaning as in Table 1.

photon radiation, Pythia is equivalent to Jetset. Thus, the Rathsman-CR model is effectively a version of Jetset which contains color reconnection. We note the Pythia Monte Carlo contains its own color reconnection model, based on the work of Khoze and Sjöstrand [29]. We do not include this model in our study because it is not implemented for Z^0 decays. The Rathsman-CR model has been found to provide a good description of rapidity gap measurements in both electron-proton and proton-antiproton collisions [30].

The parameters we use for the Ariadne-CR model are the same as those given in Table 2 for Ariadne except for the parameter PARJ(42) which was adjusted from 0.63 to 0.55 GeV^{-2} so that the model describes the measured value of mean charged particle multiplicity in inclusive Z^0 decays, $\langle n_{\mathrm{ch.}} \rangle$, see Sect. 4. Analogously, the parameters of the Herwig-CR model are the same as those used for Herwig (see Table 1) except CLMAX was adjusted from 3.35 to 3.75 GeV/c^2 and RMASS(13) from 0.75 to 0.793 GeV/c^2 to describe $\langle n_{\mathrm{ch.}} \rangle$. For our implementation of the Rathsman-CR model, we use the parameter set given for Jetset in [23].

Besides the Jetset parameters, the Rathsman-CR model employs a parameter, denoted R_0, which is an overall suppression factor for color reconnection. The value of R_0 is not arbitrary but reflects the $1/N_{\mathrm{C}}^2$ suppression of reconnected events compared to planar events mentioned in the Introduction. For this parameter, we use $R_0 = 0.1$ as suggested in [27]. The analogous parameter in the Herwig-CR model, PRECO, is maintained at its default value of $1/N_{\mathrm{C}}^2 = 1/9$. For the Ariadne-CR model, the corresponding parameter, PARA(26), stipulates the number of distinct dipole color states. We use the default value for this parameter, PARA(26) = 9, which again corresponds to $N_{\mathrm{C}} = 3$ and the $1/N_{\mathrm{C}}^2$ suppression of reconnected processes.

Our implementations of the Ariadne-CR, Herwig-CR and Rathsman-CR models provide descriptions of the global features of e^+e^- data which are essentially equivalent to those of the corresponding models without reconnection. This is discussed in Sect. 4 below.

The Monte Carlo events are examined at two levels: the "detector level" and the "hadron level." The detector level includes initial-state photon radiation, simulation of the OPAL detector [31], and the analysis procedures described in Sect. 2. The hadron level does not include these effects and utilizes all charged and neutral particles with lifetimes greater than 3×10^{-10} s, which are treated as stable. Samples of 6 million Ariadne, Herwig and Jetset events, and 3 million Ariadne-CR, Herwig-CR and Rathsman-CR events, were processed through the detector simulation and used as the detector level samples in this study. The hadron level samples are based on 10 million Monte Carlo events for each model.

4 Model predictions for inclusive Z^0 decays

The Ariadne-CR, Rathsman-CR and Herwig-CR models yield descriptions of standard measures of properties in inclusive Z^0 data which are essentially equivalent to those provided by Ariadne, Jetset, and Herwig, respectively, as stated above. Thus, color reconnection as implemented in these models has only a small effect on the global features of inclusive e^+e^- events. To illustrate these points, we measured the following distributions using the inclusive Z^0 sample discussed in Sect. 2:

1. Sphericity, S [32];
2. Aplanarity, A [32];
3. the negative logarithm of the jet resolution scale for which an event changes from being classified as a three-jet event to a four-jet event, using the Durham jet finder [33], $-\ln(y_{34})$;
4. charged particle rapidity with respect to the thrust axis, y_T.

Note there are correlations between these variables and between different bins of some of the distributions. Using a sample of Jetset events at the hadron level, the correlation coefficient between S and A was found to be 0.66, between S and $-\ln(y_{34})$ -0.61, and between A and $-\ln(y_{34})$ -0.66. Similar results were found using the other models. The y_T distribution contains one entry per particle, in contrast to the other distributions which contain one entry per event. Therefore, the y_T distribution was not included in this correlation study. Taken together, the four distributions are sensitive to the momentum structure of an event both in and out of the three-jet event plane, to four-jet event structure, and to particle multiplicity. They therefore provide a relatively complete and relatively uncorrelated set of distributions with which to assess the global features of e^+e^- events.

The distributions were corrected to the hadron level using bin-by-bin factors. The method of bin-by-bin corrections is described in [32]. Ariadne was used to determine the correction factors. Ariadne was chosen because it was found to provide a better description of the data at the detector level than Jetset or Herwig. The typical size of the corrections is 10%. As systematic uncertainties, we considered the following.

- The other models – Jetset, Herwig, Ariadne-CR, Herwig-CR and Rathsman-CR – were used to determine the correction factors, rather than Ariadne.
- Charged tracks alone were used for the data and Monte Carlo samples with detector simulation, rather than charged tracks plus electromagnetic clusters.
- The particle selection was further varied, first by restricting charged tracks and electromagnetic clusters to the central region of the detector, $|\cos\theta| < 0.70$, rather than $|\cos\theta| < 0.96$ for the charged tracks and $|\cos\theta| < 0.98$ for the clusters, and second by increasing the minimum transverse momentum of charged tracks with respect to the beam axis from 0.05 GeV/c to 0.15 GeV/c.

The differences between the standard results and those found using each of these conditions were used to define symmetric systematic uncertainties. For the first item, the largest of the described differences with respect to the standard result was assigned as the systematic uncertainty, and similarly for the third item. The systematic uncertainties were added in quadrature to define the total systematic uncertainties. The systematic uncertainty evaluated for each bin was averaged with the results from its two neighbors to reduce the effect of bin-to-bin fluctuations. The single neighbor was used for bins at the ends of the distributions.

The largest contribution to the systematic uncertainty of the S, $-\ln(y_{34})$ and y_T distributions arose from using the Herwig-CR model to correct the data. For A, the largest systematic effect was from using Jetset to correct the data.

Model (Number of bins)	S (19)	A (15)	$-\ln(y_{34})$ (26)	y_T (21)	Total (81)	$\langle n_{\mathrm{ch.}} \rangle$
Ariadne	1.7	6.8	10.7	17.7	36.9	21.06
Ariadne-CR	6.2	5.9	4.3	16.0	32.4	21.09
Jetset	18.4	91.4	64.1	26.8	200.7	21.09
Rathsman-CR	18.5	103.6	74.7	46.7	243.5	20.80
Herwig	19.3	27.0	42.5	39.1	127.9	21.14
Herwig-CR	10.5	15.7	30.6	94.8	151.6	21.06
Re-tuned Ariadne-CR ($p_{T,\mathrm{min.}} = 4.7$ GeV/$c, b = 0.17$ GeV^{-2})	498.1	548.7	1001.3	971.2	3019.3	21.12
Re-tuned Rathsman-CR ($Q_0 = 5.5$ GeV/$c^2, b = 0.27$ GeV^{-2})	106.8	294.2	429.7	287.0	1117.7	21.16

Table 3: χ^2 values between the data and models for the distributions shown in Figs. 2–5, calculated using the full experimental uncertainties including systematic terms. The number of bins in each distribution is given in parentheses in the second row. The last two rows give the results for re-tuned versions of the Ariadne-CR and Rathsman-CR models, see Sect.7.4. The models' predictions for the mean charged particle multiplicity in inclusive Z^0 decays, $\langle n_{\mathrm{ch.}} \rangle$, are listed in the last column.

The corrected measurements of S, A, $-\ln(y_{34})$ and y_T are presented in Figs. 2–5. These data are consistent with our previously published results [32]. The data are shown in comparison to the predictions of the models at the hadron level. The model predictions are generally seen to be similar to each other and in agreement with the experiment. Parts (b) and (c) of Figs. 2–5 show the deviations of the Monte Carlo predictions from the data in units of the total experimental uncertainties "σ_{data}," with statistical and systematic terms added in quadrature. The statistical uncertainties are negligible compared to the systematic uncertainties. The curves labelled "Re-tuned Rathsman-CR" and "Re-tuned Ariadne-CR" in parts (b) and (c) are discussed in Sect. 7.4.

We calculated the χ^2 values between the hadron level predictions of the models and the corrected data. The χ^2 values were determined using the total experimental uncertainties, with no accounting for correlations between the different bins or distributions. The χ^2 results are listed in Table 3. These χ^2 values are intended to be used only as a relative measure of the description of the data by the models. Since the uncertainties are dominated by systematics and correlations are not considered, these χ^2 values cannot be used to determine confidence levels assuming the uncertainties are distributed according to a normal distribution. In particular, a good description does not imply that a model's χ^2 should approximately equal the number of data bins.

From Table 3, it is seen that the χ^2 results for Ariadne are much smaller than for Jetset or Herwig. The reason for this is partly that the detector level distributions are better described by Ariadne, as stated above, and partly that Ariadne is used to determine the correction factors.

It is unavoidable that the correction procedure introduces a bias towards the model used to perform the corrections, as discussed for example in [32]. These biases – although small – can have a significant effect on the χ^2 values because of the small experimental uncertainties. For this reason, it is only meaningful to compare our χ^2 results within the context of a specific parton shower and hadronization scheme, e.g. Ariadne with Ariadne-CR but not Ariadne with Jetset.

The total χ^2 for the Ariadne-CR model is seen to be about the same as for Ariadne (in fact it is a little smaller). For the Herwig-CR model, the total χ^2 is about 20% larger than for Herwig. From Table 3, it is seen that this difference arises entirely from a single distribution, y_T, however. Similarly, the total χ^2 for the Rathsman-CR model is about 20% larger than for Jetset, with the largest contribution to the increase from y_T.

The last column in Table 3 lists the predictions of the models for the mean value of charged particle multiplicity, $\langle n_{\mathrm{ch.}} \rangle$. The statistical uncertainties are negligible. The results of all models agree with the LEP-averaged result for Z^0 decays, $\langle n_{\mathrm{ch.}} \rangle = 21.15 \pm 0.29$ [34], to within the uncertainties.

Thus the three models with color reconnection yield overall descriptions of the global properties of hadronic Z^0 events which are essentially equivalent to those of the corresponding models without reconnection. For the Ariadne-CR and Rathsman-CR models, this agrees with the observations in [25] and [27], respectively.

5 Gluon jet selection

To define jets, we use the Durham jet finder [33]. The resolution scale, y_{cut}, is adjusted separately for each event so that exactly three jets are reconstructed. The jets are assigned energies using the technique of calculated energies with massive kinematics, see for example [11]. This method relies primarily on the angles between jets and the assumption of energy-momentum conservation. Jet energies determined in this manner are more accurate than visible jet energies, with the latter defined by a sum over the reconstructed energies of the particles assigned to the jet.

To identify which of the three jets is the gluon jet, we reconstruct displaced secondary vertices in the quark (q or $\overline{\mathrm{q}}$) jets and thereby anti-tag the gluon jet. Displaced secondary vertices are associated with heavy quark decay, especially that of the b quark. At LEP, b quarks are produced almost exclusively at the electroweak vertex[4]: thus a jet containing a b hadron is almost always a quark jet. To reconstruct secondary vertices in jets, we employ the method described in [36]. Briefly, charged tracks are selected for the secondary vertex reconstruction procedure if they are assigned to the jet by the jet finder, have coordinate information from at least one of the two silicon detector layers, a momentum larger than 0.5 GeV/c, and a distance of closest approach to the primary event vertex [36] less than 0.3 cm. In addition, the uncertainty on the distance of closest approach must be less than 0.1 cm. A secondary vertex is fitted using the so-called "tear down" method [36] and is required to contain at least three

[4]About 22% of hadronic Z^0 events contain a $\mathrm{b\overline{b}}$ quark pair from the electroweak decay of the Z^0, compared to only about 0.3% [35] with a $\mathrm{b\overline{b}}$ pair from gluon splitting.

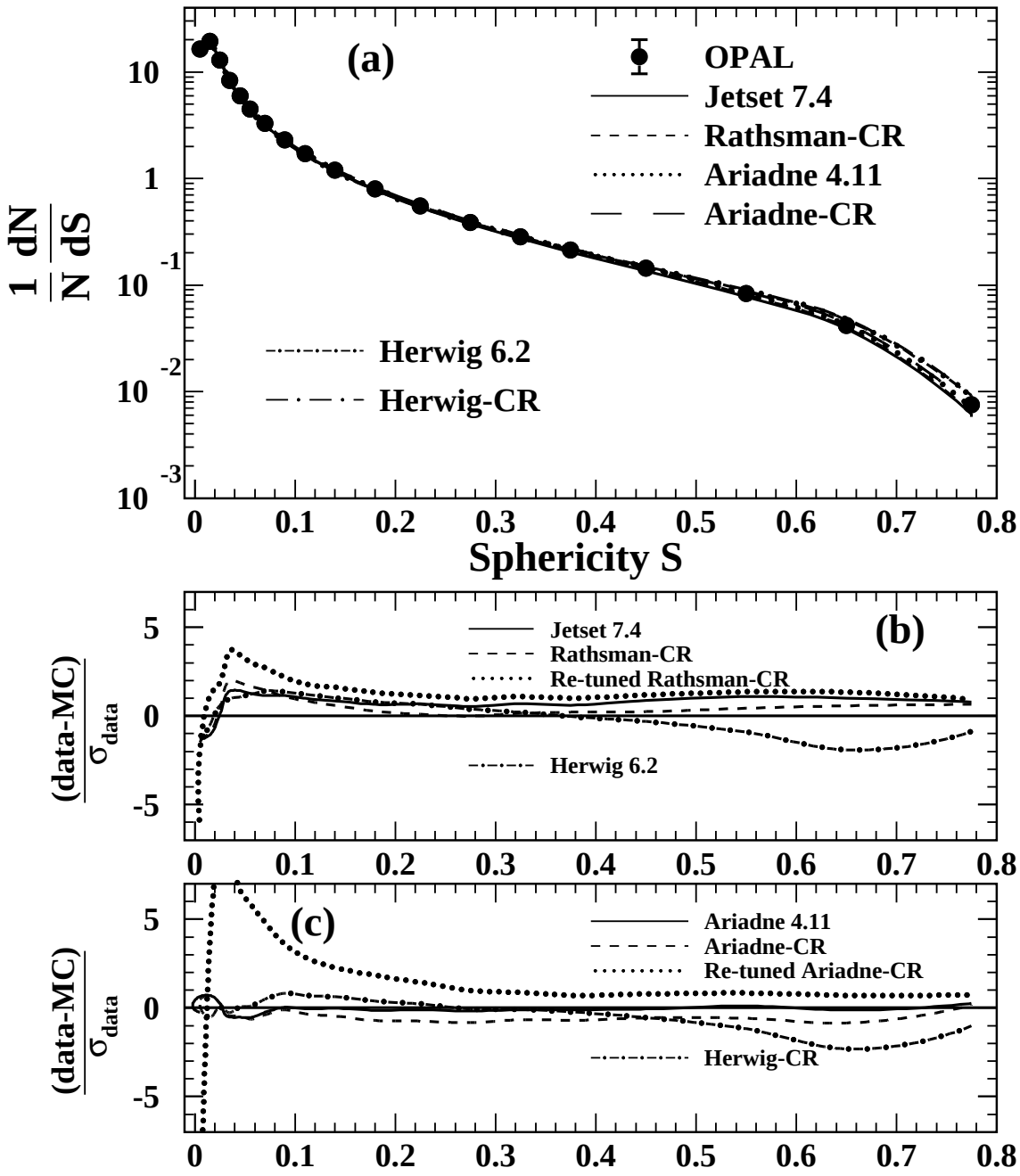

Figure 2: (a) The Sphericity distribution for inclusive Z^0 events, in comparison to the predictions of models with and without color reconnection (CR). The data have been corrected for initial-state photon radiation and detector response. The statistical uncertainties are too small to be visible. The vertical lines attached to the data points (barely visible) show the total uncertainties, with statistical and systematic terms added in quadrature. (b) and (c) show the deviations of the Monte Carlo predictions from the data in units of the total experimental uncertainties, $\sigma_{\rm data}$.

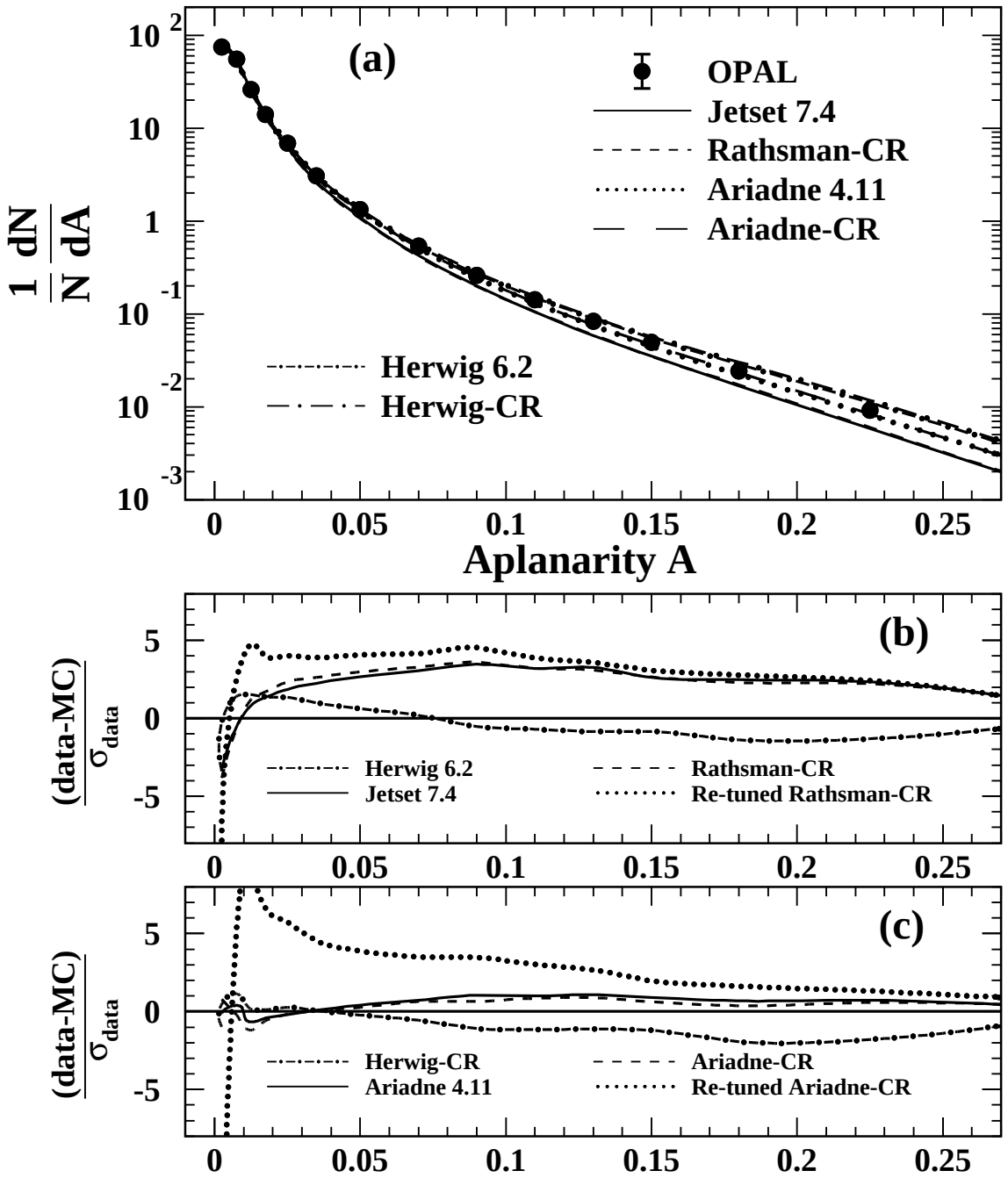

Figure 3: (a) The Aplanarity distribution for inclusive Z^0 events, in comparison to the predictions of models with and without color reconnection (CR). The data have been corrected for initial-state photon radiation and detector response. The uncertainties – both statistical and total – are too small to be visible. (b) and (c) show the deviations of the Monte Carlo predictions from the data in units of the total experimental uncertainties, $\sigma_{\rm data}$.

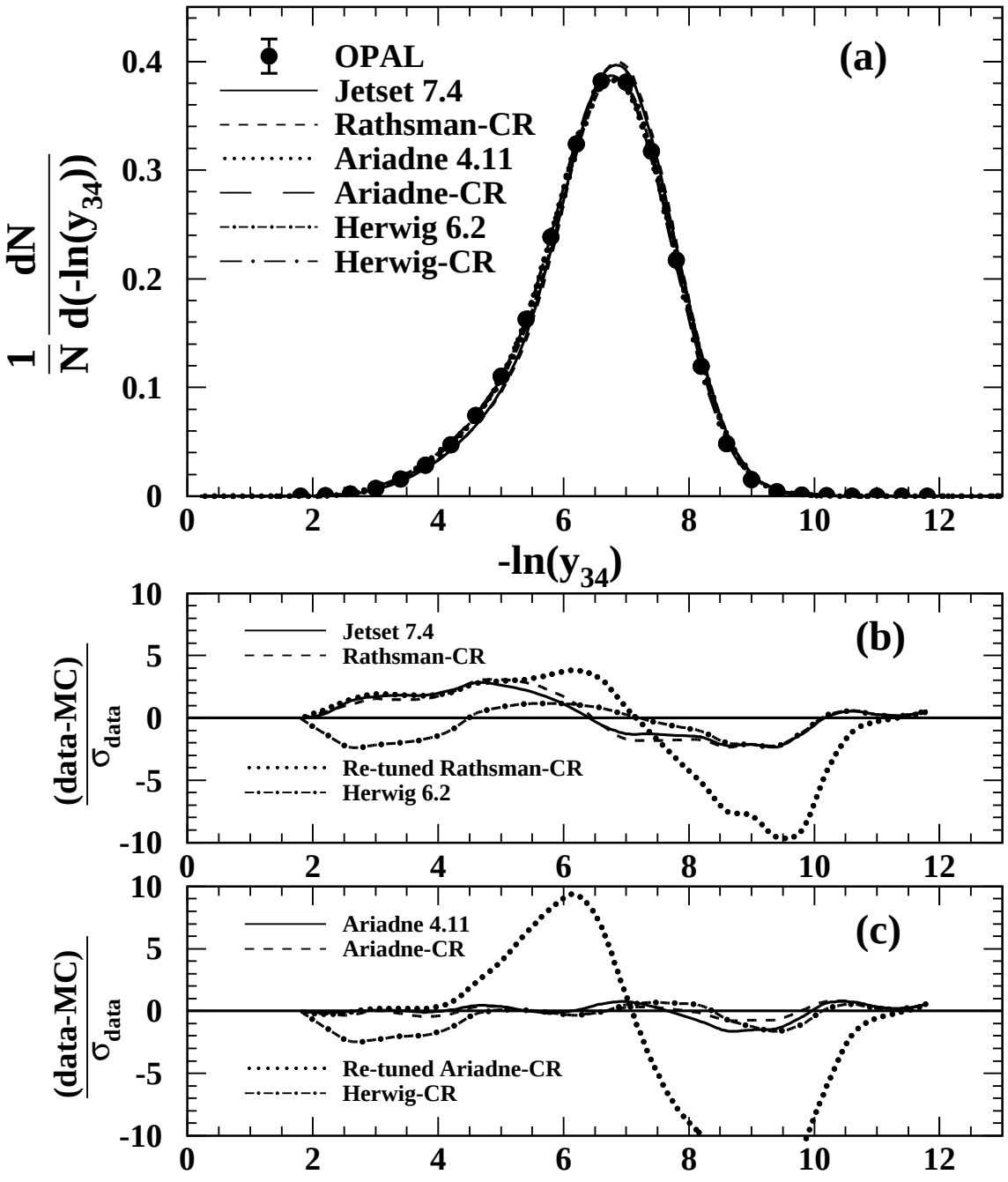

Figure 4: (a) The $-\ln(y_{34})$ distribution for inclusive Z^0 events, in comparison to the predictions of models with and without color reconnection (CR). The data have been corrected for initial-state photon radiation and detector response. The uncertainties – both statistical and total – are too small to be visible. (b) and (c) show the deviations of the Monte Carlo predictions from the data in units of the total experimental uncertainties, $\sigma_{\rm data}$.

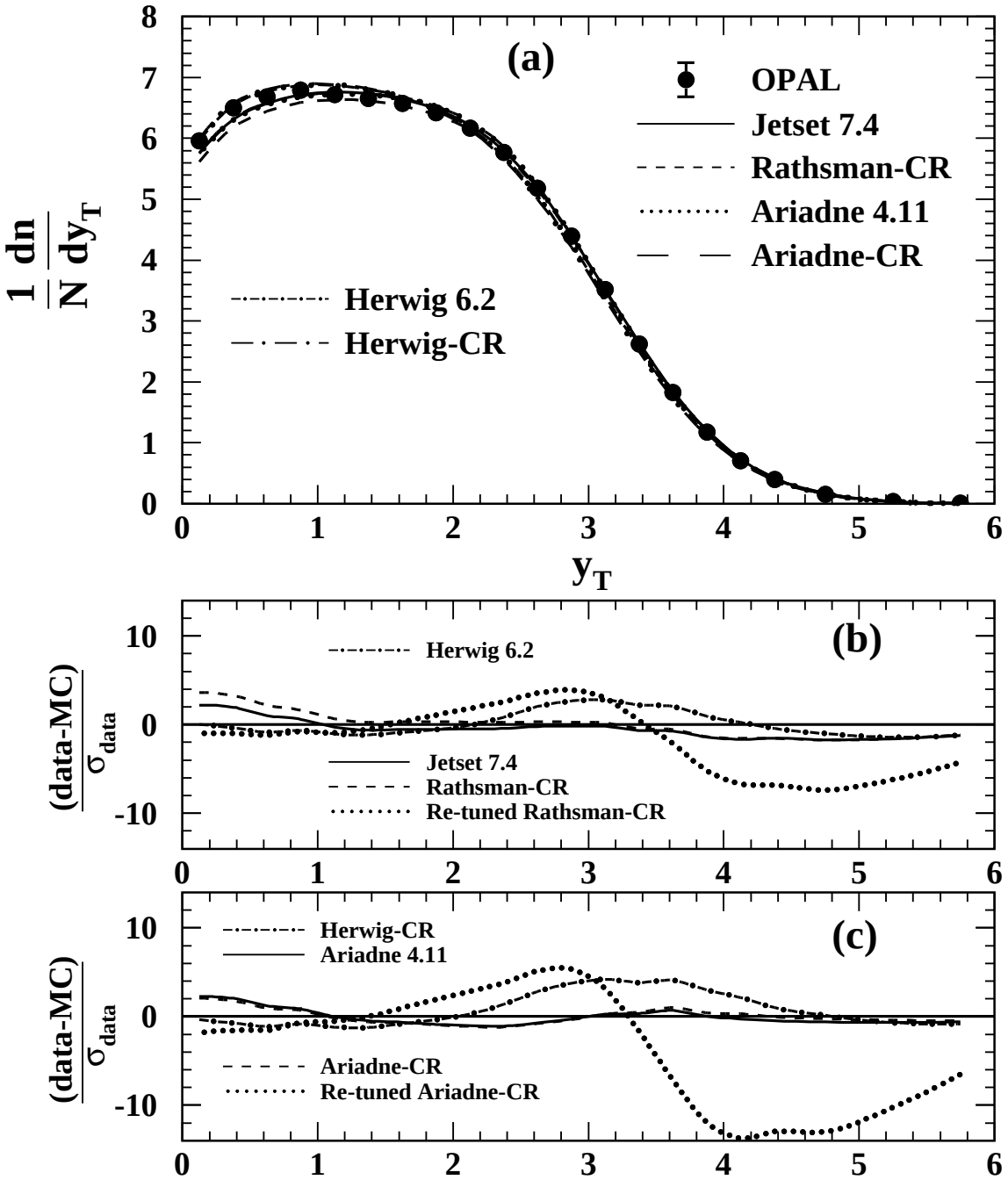

Figure 5: (a) The y_T distribution for inclusive Z^0 events, in comparison to the predictions of models with and without color reconnection (CR). The data have been corrected for initial-state photon radiation and detector response. The uncertainties – both statistical and total – are too small to be visible. (b) and (c) show the deviations of the Monte Carlo predictions from the data in units of the total experimental uncertainties, $\sigma_{\rm data}$.

such tracks. For jets with such a secondary vertex, the signed decay length, L, is calculated with respect to the primary vertex, along with its error, σ_L. The sign of L is determined by summing the 3-momenta of the tracks fitted to the secondary vertex; $L > 0$ if the secondary vertex is displaced from the primary vertex in the same hemisphere as this momentum sum, and $L < 0$ otherwise. To be identified as a quark jet, a jet is required to have a successfully reconstructed secondary vertex with $L/\sigma_L > 2.0$ if it is the highest energy jet or $L/\sigma_L > 5.0$ if it is one of the two lower energy jets. We require the highest energy jet and exactly one of the two lower energy jets to be identified as quark jets. The other lower energy jet is tagged as a gluon jet.

For each tagged gluon jet, we determine the scale, $\kappa_{\rm jet}$, given by

$$\kappa_{\rm jet} = E_{\rm jet} \, \sin\left(\frac{\theta_{\rm min.}}{2}\right) \tag{1}$$

where $E_{\rm jet}$ is the energy of the jet, with $\theta_{\rm min.}$ the smaller of the angles between the gluon jet and the other two jets. Note that due to QCD coherence, the properties of a gluon jet in $\rm e^+e^-$ annihilations depend on a transverse momentum-like quantity such as $\kappa_{\rm jet}$ and not the jet energy, see for example [37]. $\kappa_{\rm jet}$ as defined in eq. (1) was shown to be an appropriate scale for gluon jets in [38].

The $\kappa_{\rm jet}$ distribution of the tagged gluon jets is shown in Fig. 6. The data are presented in comparison to the predictions of the detector level QCD models introduced in Sect. 3. All the simulations are seen to provide a good description of the measured $\kappa_{\rm jet}$ spectrum.

To select hard, acollinear gluon jets, we require $\kappa_{\rm jet} \geq 7$ GeV. Further, we require the energy of the gluon jets to be less than 35 GeV because the simulations predict the gluon jet purity (see below) drops sharply for higher energies. The jets are required to contain at least two particles. With these cuts, the number of selected gluon jets is 12 611. The energy of the jets varies from about 10 GeV up to the cutoff of 35 GeV, with an average and RMS of 21.7 GeV and 6.6 GeV, respectively.

To evaluate the purity of the gluon jets, we use Monte Carlo samples at the detector level. We determine the directions of the primary quark and antiquark from the $\rm Z^0$ decay after the parton shower has terminated. The detector level jet closest to the direction of an evolved primary quark or antiquark is considered to be a quark jet. The distinct jet closest to the evolved primary quark or antiquark not associated with this first jet is considered to be the other quark jet. The remaining jet is the gluon jet. The estimated gluon jet purity found using Jetset is approximately constant at 98% for jet energies from 10 to 25 GeV, then decreases to 78% at 35 GeV. The overall purity is $(94.6 \pm 0.1\,(\text{stat.}))\%$. Similar results are obtained using all other models except for Ariadne-CR.[5] Note the overall purity of the gluon jets decreases to 86% after the requirement of a rapidity gap is imposed, see Sect. 6. The reason the purity is lower if a rapidity gap is required is because gluon jets have a larger mean multiplicity than quark jets [39], making it less likely a gap will occur in gluon jets compared to quark jets as the result of a fluctuation. By requiring the presence of a rapidity gap, the relative proportion of quark jets is therefore enhanced.

[5]For the Ariadne-CR model, the estimated purity is smaller, about 72%. Since this model does not describe our gluon jet measurements well (see Sect. 7), it is not clear if this estimate is reliable, however. Note the estimates of gluon jet purity are presented for informational purposes only.

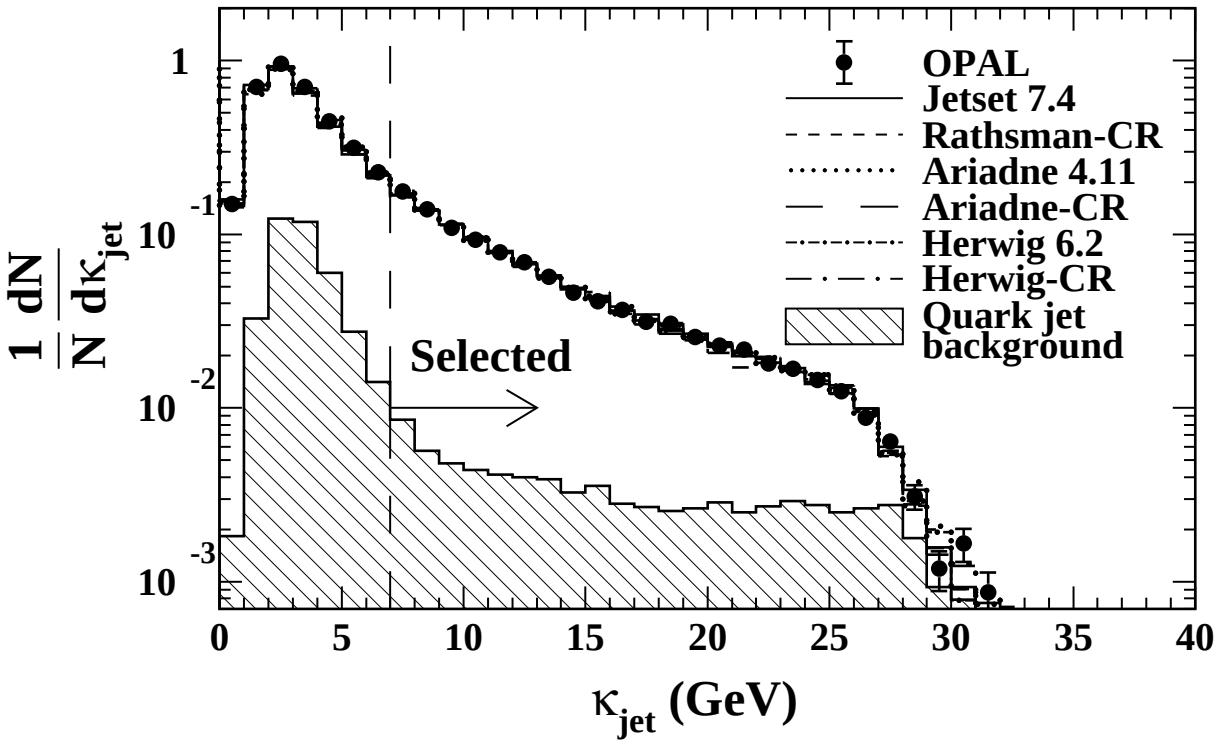

Figure 6: Distribution of the $\kappa_{\rm jet}$ scale of tagged gluon jets, see eq. (1). The distribution includes the effects of initial-state photon radiation and detector acceptance and resolution. The uncertainties are statistical only. The results are shown in comparison to the predictions of QCD Monte Carlo programs which include detector simulation and the same analysis procedures as are applied to the data. To define hard, acollinear gluon jets, the region $\kappa_{\rm jet} \geq 7$ GeV, to the right of the vertical dashed line, is selected. The hatched area shows the quark jet background evaluated using Jetset.

6 Rapidity gap analysis

To identify gluon jets with a rapidity gap, we examine the charged and neutral particles assigned to the selected gluon jets by the jet finder. The rapidities of the particles are determined with respect to the jet axis. The particles in the jet are ordered by their rapidity values.

Models with color reconnection are expected to yield more events with a large rapidity gap than models without reconnection, as discussed in the Introduction. A large rapidity gap can correspond to a large value for the smallest particle rapidity in a jet, $y_{\rm min}$, or else to a large value for the maximum difference between the rapidities of adjacent rapidity-ordered particles, $\Delta y_{\rm max}$. These two types of rapidity gap conditions are illustrated schematically in Fig. 7. Note that the Durham jet finder occasionally assigns particles to a jet even if the angle between the particle and jet axis is greater than 90°. This explains the negative rapidity values illustrated for some particles in Fig. 7b.

The measured distribution of $y_{\rm min}$ is presented in Fig. 8a. The data are shown in comparison to the predictions of the models at the detector level. To emphasize the difference between

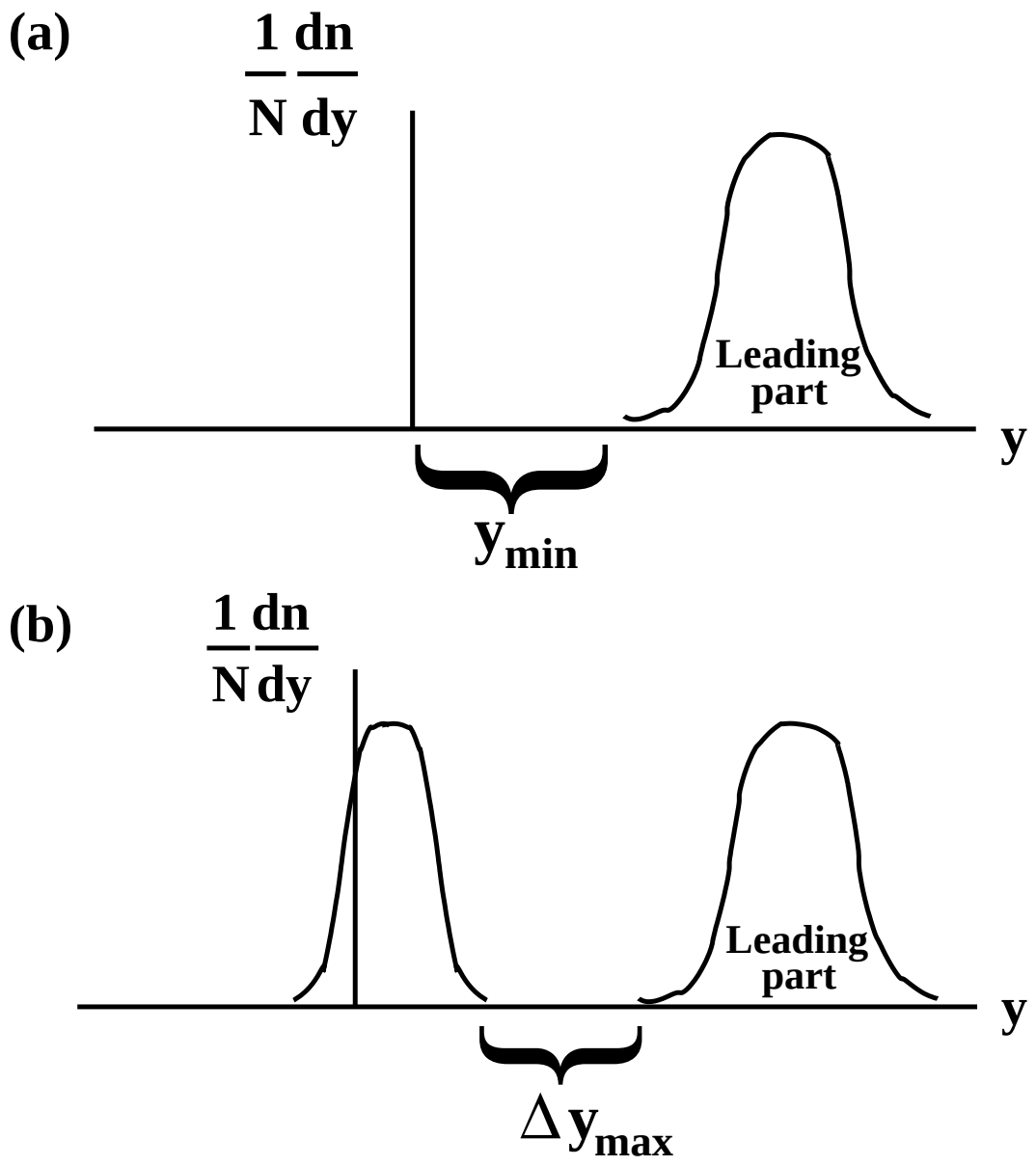

Figure 7: Schematic illustration of the distribution of particle rapidities for gluon jets with a rapidity gap as defined in this study: (a) for the $y_{\min}$ sample (see text), and (b) for the $\Delta y_{\max}$ sample. The leading parts of the gluon jets are defined by charged and neutral particles with rapidities beyond the gap, as indicated in the figure.

models with and without color reconnection, we form the following ratio:

$$\delta_{y_{\min}} = \frac{f(y_{\min})_{\mathrm{CR}} - f(y_{\min})_{\mathrm{no\,CR}}}{f(y_{\min})_{\mathrm{no\,CR}}} \tag{2}$$

with $f(y_{\min})_{\mathrm{CR}}$ the prediction of a model with color reconnection for a bin of the $y_{\min}$ distribution in Fig. 8a and $f(y_{\min})_{\mathrm{no\,CR}}$ the prediction of the corresponding model without reconnection. The results for $\delta_{y_{\min}}$ are shown in Fig. 8b. For the Rathsman-CR model, a significant excess of events is observed relative to Jetset for $y_{\min}$ values larger than about 1.4, and similarly for the Ariadne-CR model relative to Ariadne. The Herwig-CR model exhibits a similar excess with respect to Herwig, although with less significance. Based on these results, we choose $y_{\min} \geq 1.4$ to select a sample of gluon jets with a rapidity gap, see the dashed vertical line in Fig. 8b. In the following, we refer to this as the "$y_{\min}$" sample.

For gluon jets with $y_{\min} < 1.4$, we measure $\Delta y_{\max}$. The resulting distribution is shown in Fig. 9a. In analogy to eq. (2), we form the fractional difference $\delta_{\Delta y_{\max}}$. The distribution of $\delta_{\Delta y_{\max}}$ is shown in Fig. 9b. A significant excess of events is observed for the Ariadne-CR and Rathsman-CR models, relative to Ariadne and Jetset, for $\Delta y_{\max}$ larger than about 1.3. We therefore choose $\Delta y_{\max} \geq 1.3$ to select an additional sample of gluon jets with a rapidity gap, see the dashed vertical line in Fig. 9b. In the following, we refer to this as the "$\Delta y_{\max}$" sample. For the Herwig-CR model, there is not a clear excess of events relative to Herwig for any $\Delta y_{\max}$ value, suggesting this distribution is not sensitive to color reconnection as implemented in Herwig. In the following, we therefore test the Herwig-CR model using the $y_{\min}$ sample only, not the standard data set defined by the $y_{\min}$ and $\Delta y_{\max}$ samples taken together.

In total, 655 gluon jets with a rapidity gap are selected, 496 in the $y_{\min}$ sample and 159 in the $\Delta y_{\max}$ sample. The purity of the gluon jets, evaluated using the method described in Sect. 5, is approximately 94% for gluon jet energies between 10 and 25 GeV, then drops to about 50% at 35 GeV. The overall purity is $(85.7 \pm 1.0\,(\mathrm{stat.}))\%$. Our subsequent study is based on the leading part of these jets, defined by charged and neutral particles with $y \geq y_{\min}$ for events[6] in the $y_{\min}$ sample and by particles with rapidities beyond the gap $\Delta y_{\max}$ for events in the $\Delta y_{\max}$ sample, see Fig. 7.

7 Color reconnection study

To remain as sensitive as possible to color reconnection, we first compare the Monte Carlo distributions to the data at the detector level. Following this, we correct the measurements for the effects of initial-state radiation, detector acceptance and resolution, and gluon jet impurity, and compare the predictions of the models to the data at the hadron level. The hadron level study allows us to more readily assess the effect of adjusting Monte Carlo parameters, see Sect. 7.4.

The distributions presented in this section are normalized to the total number of selected gluon jets discussed in Sect. 5, i.e. to the number of gluon jets before the rapidity gap requirement. The reason for this is to remain sensitive to the rate at which gluon jets with a rapidity gap occur, e.g. to the production rate of events like Fig.1b.

[6]For events in this class, this is therefore the entire jet, see Fig. 7a.

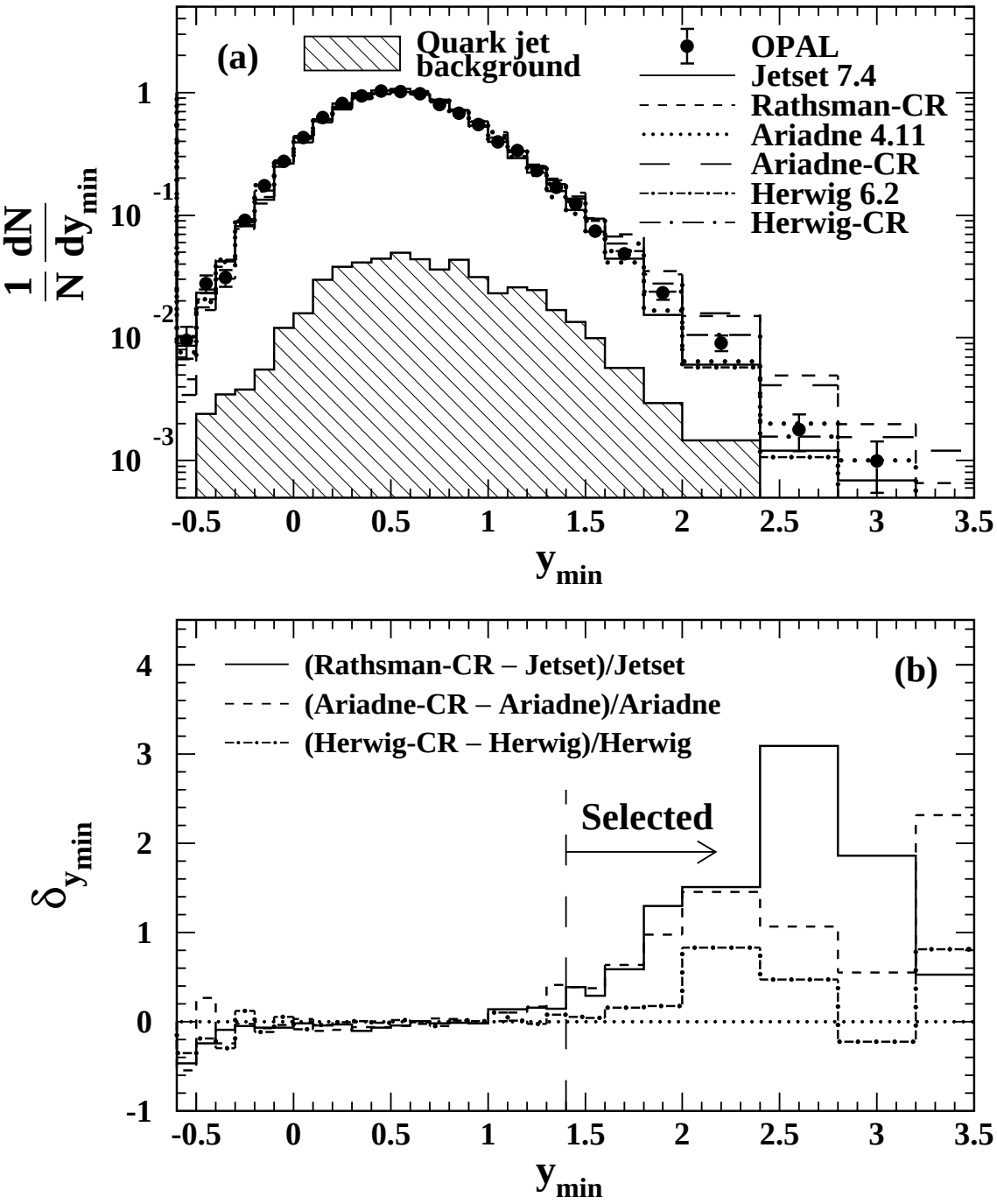

Figure 8: (a) Distribution of $y_{\min}$ in the tagged gluon jets. The distribution includes the effects of initial-state photon radiation and detector acceptance and resolution. The uncertainties are statistical only. The results are shown in comparison to the predictions of QCD Monte Carlo programs which include detector simulation and the same analysis procedures as are applied to the data. The hatched area shows the quark jet background evaluated using Jetset. (b) Fractional difference between the results of a Monte Carlo program with color reconnection and the corresponding model without reconnection. To define gluon jets with a rapidity gap, the region $y_{\min} \geq 1.4$, to the right of the vertical dashed line, is selected.

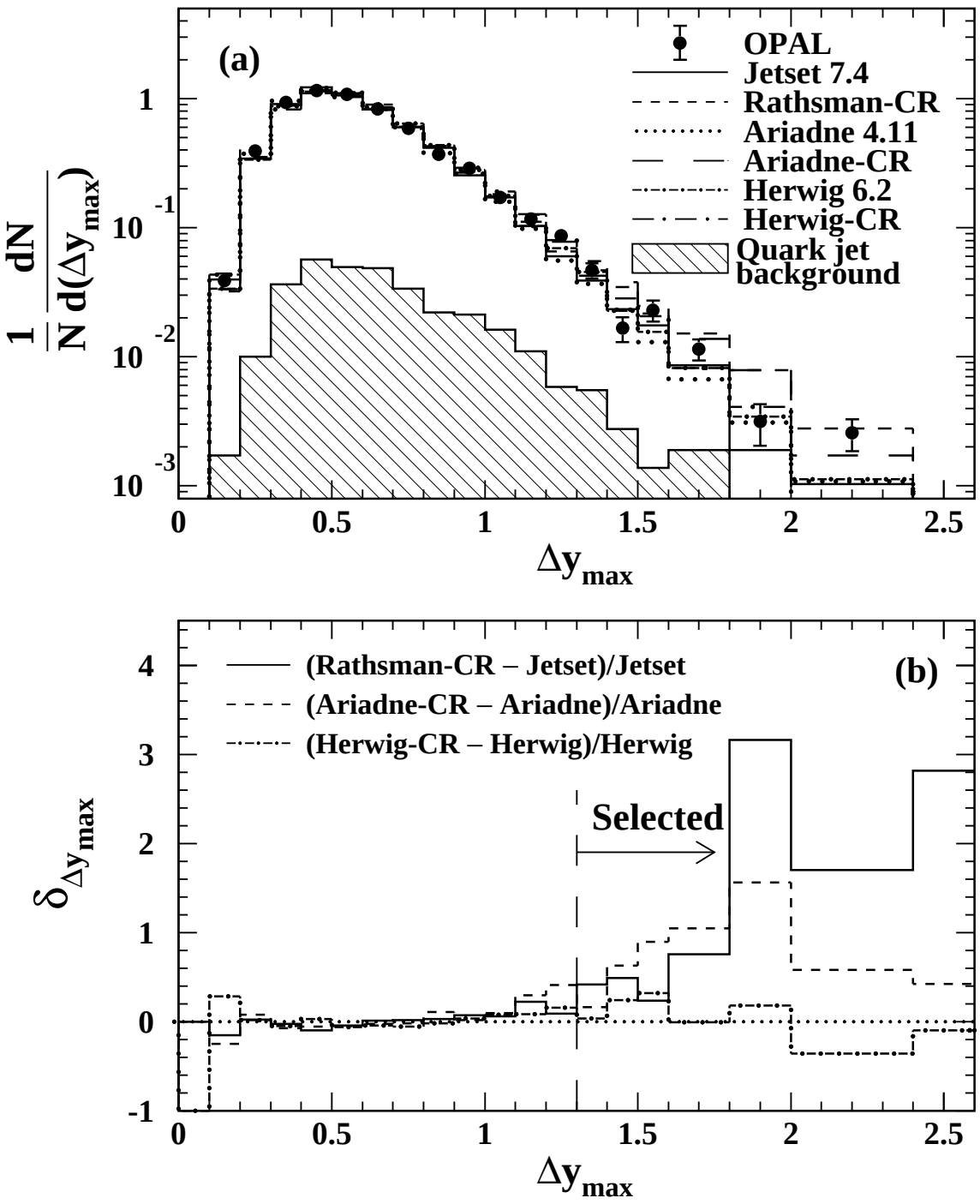

Figure 9: (a) Distribution of $\Delta y_{\max}$ for tagged gluon jets with $y_{\min} < 1.4$. The distribution includes the effects of initial-state photon radiation and detector acceptance and resolution. The uncertainties are statistical only. The results are shown in comparison to the predictions of QCD Monte Carlo programs which include detector simulation and the same analysis procedures as are applied to the data. The hatched area shows the quark jet background evaluated using Jetset. (b) Fractional difference between the results of a Monte Carlo program with color reconnection and the corresponding model without reconnection. To define gluon jets with a rapidity gap, the region $\Delta y_{\max} \geq 1.3$, to the right of the vertical dashed line, is selected.

7.1 Detector level distributions

The charged particle multiplicity distribution of the leading part of the gluon jets, $n^{\rm ch.}_{\rm leading}$, is shown in Fig. 10a. The results are shown in comparison to the predictions of the Jetset and Rathsman-CR models. Fig. 10b shows the same data compared to Ariadne and Ariadne-CR. The most striking feature of these results is the large excess of entries predicted by the Ariadne-CR and Rathsman-CR models at $n^{\rm ch.}_{\rm leading} = 2$ and 4 compared to the corresponding models without color reconnection. Using Monte Carlo information, we verified these excesses are a consequence of events like Fig. 1b, present in the CR models but not in the models without CR. The isolated, electrically neutral gluonic system in the leading part of the gluon jets in these events decays into an even number of charged particles, yielding the spikes at $n^{\rm ch.}_{\rm leading} = 2$ and 4.

The data are generally well described by Jetset (Fig. 10a), except for the bins with $n^{\rm ch.}_{\rm leading} =$ 1, 2 and 4 where the data exceed the predictions by more than one standard deviation of the statistical uncertainties. The description by Ariadne (Fig. 10b) is considerably worse in that the data lie well above the Ariadne results for most of the range between $n^{\rm ch.}_{\rm leading} = 2$ and 6. Nonetheless, Jetset and Ariadne provide a much better overall description of the data than the corresponding models with reconnection. In particular, there is not a significant "spiking effect" in the data at even values of multiplicity as predicted by these two CR models. We conclude that color reconnection as implemented by the Rathsman-CR and Ariadne-CR models is strongly disfavored, at least using their standard parameters given in Sect. 3.

The $n^{\rm ch.}_{\rm leading}$ distribution obtained using the $y_{\rm min}$ selection (see Sect. 6) is presented in Fig. 11. The data are shown in comparison to the corresponding results of the Herwig and Herwig-CR models. We use the $y_{\rm min}$ selection to test Herwig-CR, and not the standard selection defined by the combined $y_{\rm min}$ and $\Delta y_{\rm max}$ samples, because the latter is not sensitive to differences between the Herwig and Herwig-CR models as discussed in Sect. 6. For purposes of comparison, the prediction of Herwig using the standard selection is shown in Fig. 10a, however.

From Fig. 11, the Herwig-CR model is seen to predict a systematic excess of entries relative to the corresponding model without CR for multiplicities between about 2 and 5. The overall description of the $n^{\rm ch.}_{\rm leading}$ distribution by the Herwig-CR model is nonetheless reasonable, at least in comparison to the predictions of Jetset and Ariadne in Fig. 10. The best overall description of the $n^{\rm ch.}_{\rm leading}$ distribution is provided by Herwig.

We next sum the charges of the particles in the leading part of the gluon jets to find the total leading electric charge, $Q_{\rm leading}$. This type of distribution was suggested in [9]. The distribution of $Q_{\rm leading}$ is shown in Fig. 12a. The Rathsman-CR and Ariadne-CR models are seen to predict a large excess of events with $Q_{\rm leading} = 0$ compared to the data or models without reconnection, due to the presence of electrically neutral isolated gluonic systems at large rapidities as discussed above. The Jetset and Ariadne predictions for the rate of gluon jets with $Q_{\rm leading} = 0$ are about 20% too low. For purposes of comparison, the prediction of Herwig is shown in Fig. 12a. Herwig is seen to describe the data well.

Our measurement of the rate of gluon jets with $Q_{\rm leading} = 0$ therefore lies between the predictions of the Jetset and Rathsman-CR models, and similarly between the predictions of Ariadne and Ariadne-CR. In this respect, the data appear to be consistent with the presence of a fi-

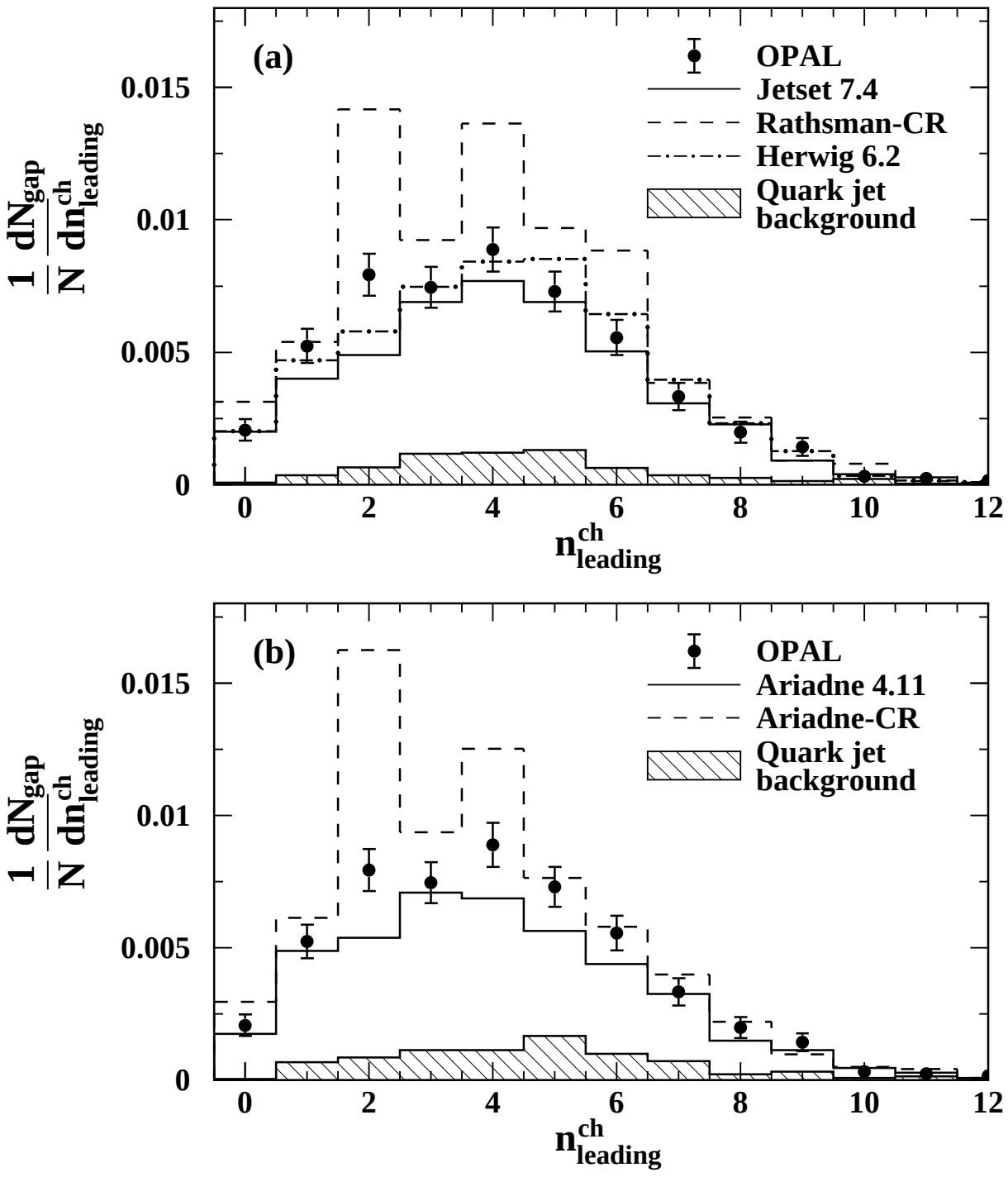

Figure 10: Distribution of $n^{\mathrm{ch.}}_{\mathrm{leading}}$ in the leading part of gluon jets, based on our standard selection. "N" represents the total number of selected gluon jets and "N_{gap}" the number of gluon jets with a rapidity gap. The distribution includes the effects of initial-state photon radiation and detector acceptance and resolution. The uncertainties are statistical only. The results are shown in comparison to the predictions of QCD Monte Carlo programs which include detector simulation and the same analysis procedures as are applied to the data: (a) the Jetset, Rathsman-CR and Herwig models, and (b) the Ariadne and Ariadne-CR models. The hatched area shows the quark jet background evaluated using Jetset in part (a) and Ariadne in part (b).

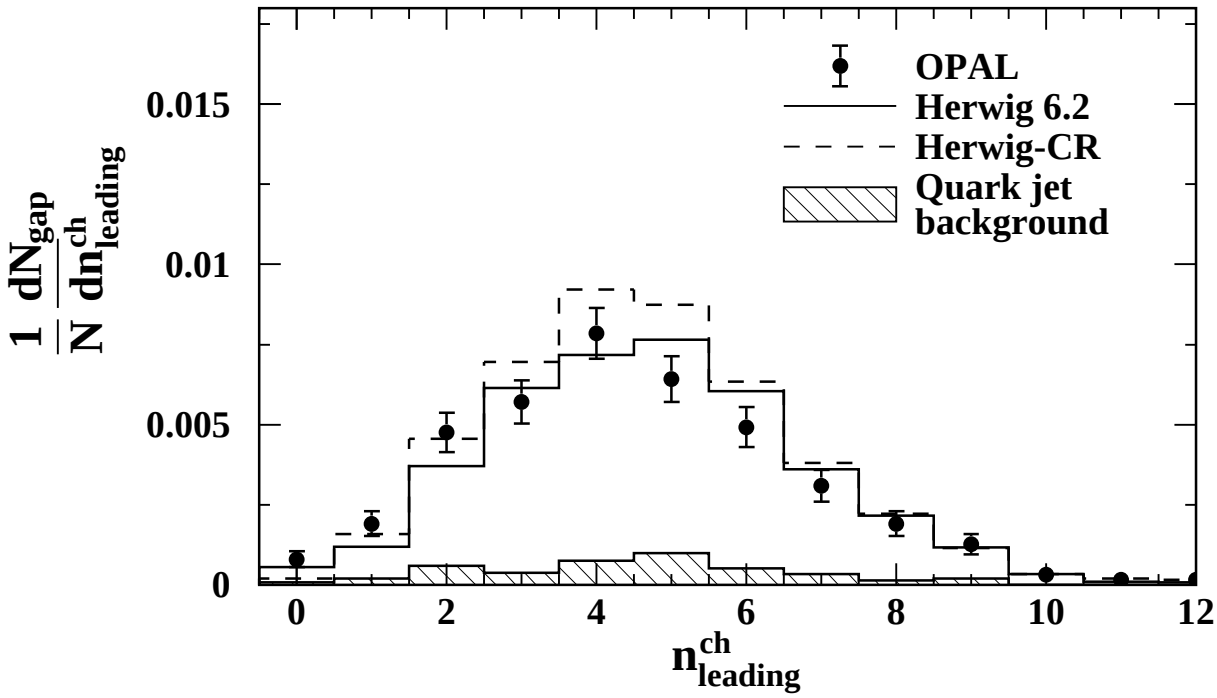

Figure 11: Distribution of $n^{\text{ch.}}_{\text{leading}}$ in the leading part of gluon jets, based on the $y_{\min}$ selection (see Sect. 6). "N" represents the total number of selected gluon jets and "N_{gap}" the number of gluon jets with a rapidity gap. The distributions include the effects of initial-state photon radiation and detector acceptance and resolution. The results are shown in comparison to the predictions of the Herwig and Herwig-CR models. The uncertainties are statistical only. The hatched area shows the quark jet background evaluated using Herwig.

nite amount of color reconnection, at least as predicted by these two CR models, albeit at a significantly smaller level than predicted by the default CR settings of the models. The most unambiguous signal for color reconnection in our study is the spiking effect at even values of $n^{\text{ch.}}_{\text{leading}}$ seen in Fig. 10, however. The data do not provide clear evidence for these spikes. Furthermore, the Herwig model without CR describes the Q_{leading} distribution well, as seen from Fig. 12a. Therefore, the discrepancies of Jetset and Ariadne with the data in Fig. 12a do not provide unambiguous evidence for reconnection effects, but instead are consistent with other inadequacies in the simulations, not related to CR. The same statement holds for the discrepancies of Jetset and Ariadne with the data in Fig. 10.

The distribution of Q_{leading} obtained using the $y_{\min}$ selection is presented in Fig. 12b. The data are shown in comparison to the corresponding results from Herwig and Herwig-CR. Herwig describes the data well, similar to Fig. 12a. The predictions of the Herwig-CR model are seen to lie somewhat above the data, especially for $Q_{\text{leading}} = 0$ and 1.

As a systematic check, we repeated the analysis presented above using different choices for the scale of gluon jets, κ_{jet}, see eq. (1). Specifically we examined the results for $4 < \kappa_{\text{jet}} < 7$ GeV and $\kappa_{\text{jet}} < 4$ GeV, rather than $\kappa_{\text{jet}} > 7$ GeV as in our standard analysis. Note the definition of a gluon jet becomes ambiguous for small κ_{jet} values. We find that the spikes at even values of $n^{\text{ch.}}_{\text{leading}}$ predicted by the Rathsman-CR and Ariadne-CR models become much less prominent

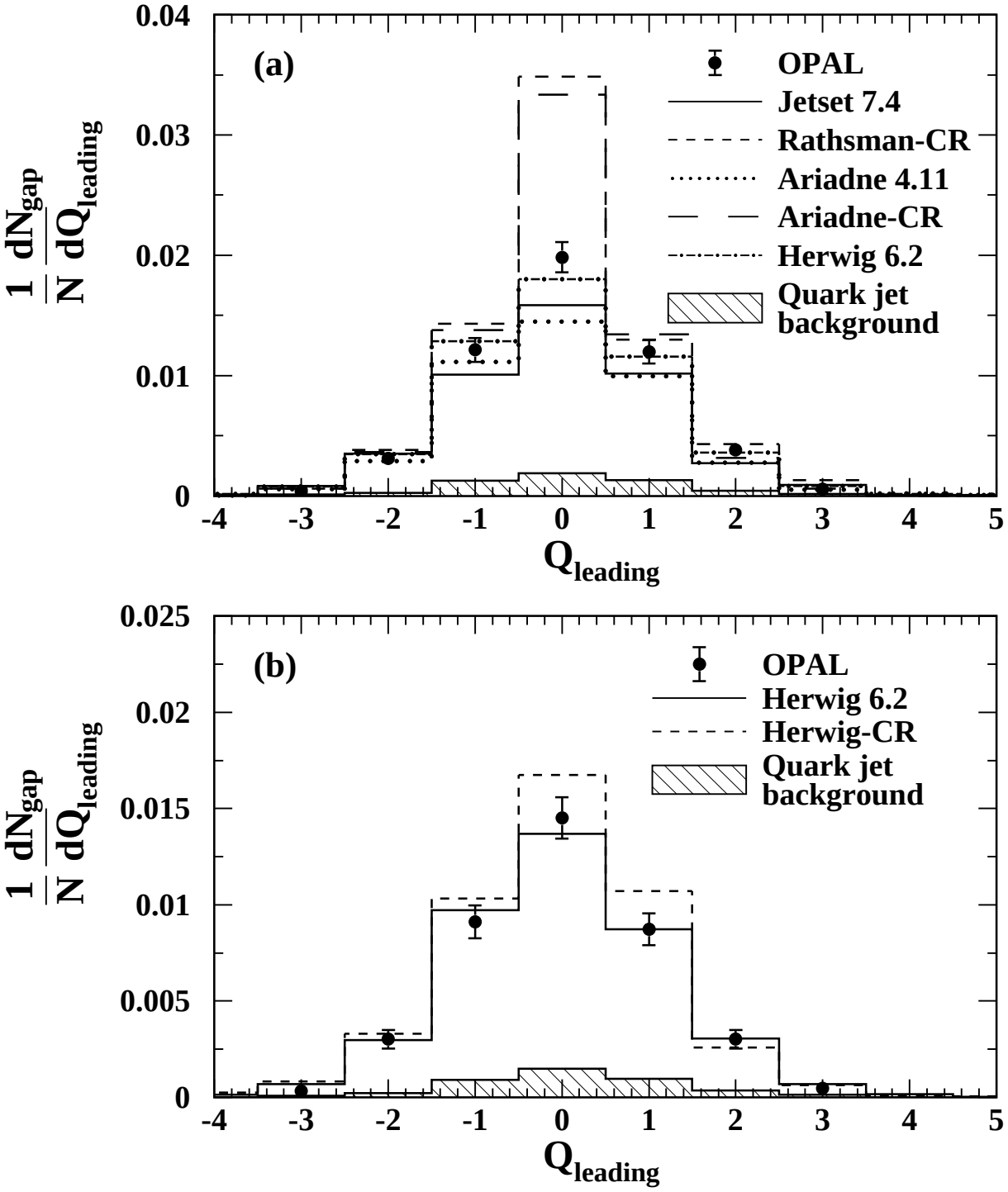

Figure 12: Distribution of Q_{leading} in the leading part of gluon jets in comparison to the predictions of QCD Model Carlo programs: (a) using the standard selection; (b) using the $y_{\min}$ selection. "N" represents the total number of selected gluon jets and "N_{gap}" the number of gluon jets with a rapidity gap. For both parts (a) and (b), the distributions include the effects of initial-state photon radiation and detector acceptance and resolution. The uncertainties are statistical only. The hatched area shows the quark jet background evaluated using Herwig.

for the smaller $\kappa_{\rm jet}$ scales, especially the spike at $n^{\rm ch.}_{\rm leading} = 4$, i.e. the selections with softer or more collinear gluon jets are less sensitive to color reconnection. This justifies the choice $\kappa_{\rm jet} > 7$ GeV for our standard analysis. To the extent that a CR signal is still visible using the smaller $\kappa_{\rm jet}$ ranges, we find that the values of $y_{\rm min}$ and $\Delta y_{\rm max}$ above which the predictions of the CR models exhibit deviations from the non-CR models are similar to those shown in Figs. 8b and 9b.

As an additional check, we repeated the analysis described in Sects. 5 and 6 except using energy ordering to identify gluon jets rather than secondary vertex reconstruction. In the energy ordering method, the jet with the smallest calculated energy in three-jet $q\overline{q}g$ events is assumed to be the gluon jet. The purity of gluon jets identified using this technique is much lower than found using secondary vertices, especially for the high energy jets most sensitive to color reconnection. The gluon jet purity found using energy ordering is 64%, compared to 95% for our standard analysis. To increase the purity, we therefore required $E_{\rm jet} < 15$ GeV, rather than $E_{\rm jet} < 35$ GeV as in the standard analysis. This method yields about 94 000 tagged gluon jets. The mean gluon jet energy is 12.9 GeV and the estimated purity 81%. After imposing the rapidity gap requirements of Sect. 6, we obtain 6604 gluon jets with an estimated purity of 56%. The results we obtain from this check are consistent with our observations presented above. In particular, the results for the $Q_{\rm leading}$ distribution are qualitatively similar to those shown in Fig. 12. We note, however, that the spike at $n^{\rm ch.}_{\rm leading} = 4$ predicted by the Rathsman-CR and Ariadne-CR models in Fig. 10 is not visible in the corresponding Monte Carlo predictions based on energy ordering, because of their softer energy scales (i.e. this is similar to the check employing smaller $\kappa_{\rm jet}$ values, mentioned above). Therefore the selection using energy ordering is not as sensitive to color reconnection as our standard selection.

The results of Figs. 10–12 demonstrate the sensitivity of our study to processes with color reconnection. We discuss the effect of parameter variation on the predictions of the Rathsman-CR and Ariadne-CR models in Sect. 7.4.

7.2 Correction procedure

As the next step in our study, we correct the data in Figs. 10–12 to the hadron level. The correction procedure employs an unfolding matrix. The matrix is constructed using detector level Monte Carlo events. The events are subjected to the detector level requirements of Sects. 2 and 5. In addition, the events are required to exhibit a rapidity gap, defined by the conditions of Sect. 6, at both the detector and hadron levels. The matrices relate the values of $n^{\rm ch.}_{\rm leading}$ and $Q_{\rm leading}$ at the detector level to the corresponding values before the same event is processed by the detector simulation. Thus the matrices correct the data to the hadron level with the exception that initial-state radiation and the experimental event acceptance are included. In a second step, the data are corrected for event acceptance, initial-state radiation, and gluon jet impurity using bin-by-bin factors. The matrices and bin-by-bin factors are determined using Herwig because the data in Figs. 10–12 are best described by that model. Statistical uncertainties are evaluated for the corrected data using propagation of errors, including the statistical uncertainties of the correction factors.

Because of finite acceptance, especially for soft particles, significantly more events satisfy the rapidity gap requirements at the detector level than at the hadron level. As a consequence, the

overall corrections are fairly large, of the order of 40%. To verify the reliability of the correction procedure, we therefore performed the following test. We treated our sample of Jetset events at the detector level as "data," using the Herwig derived corrections to unfold them. The corrected Jetset distributions were found to agree with the corresponding Jetset distributions generated at the hadron level to within the statistical uncertainties. This demonstrates that our correction procedure does not introduce a significant bias.

To evaluate systematic uncertainties for the corrected data, we repeated the analysis using the three systematic variations listed in Sect. 4, with one exception: to determine the systematic uncertainty related to the model dependence of the correction factors, we repeated the analysis using the Jetset, Ariadne and Herwig-CR models only. We did not include the Rathsman-CR or Ariadne-CR model because of their poor description of the data, see Figs. 10 and 12a. In addition, we made the following change to the standard analysis to assess the effect of altering the criteria used to identify gluon jets.

- To identify the lower energy quark jets, we required the decay length to satisfy $L/\sigma_L > 3$ rather than $L/\sigma_L > 5$; this resulted in 1002 tagged gluon jets which satisfied the rapidity gap requirements, with an estimated purity of 76%.

The systematic uncertainties were treated as described in Sect. 4, i.e. the full differences of the results of the systematic checks with respect to the standard analysis defined the systematic uncertainty for each term, and the individual terms were added in quadrature to define the total systematic uncertainties.

The largest contributions to the total systematic uncertainties arose from using Ariadne to determine the correction factors, followed by the requirement $L/\sigma_L > 3$ to identify the lower energy quark jets.

7.3 Hadron level distributions

The corrected distributions of $n^{\rm ch.}_{\rm leading}$ and $Q_{\rm leading}$ are presented in Fig. 13. These results are based on our standard selection, i.e. the $y_{\rm min}$ and $\Delta y_{\rm max}$ samples added together. The data are shown in comparison to the hadron level predictions of the Jetset, Rathsman-CR, Ariadne and Ariadne-CR models. For purposes of comparison, the predictions of Herwig are shown as well. The qualitative features of the predictions are seen to be similar to those of the corresponding detector level distributions in Figs. 10 and 12a. In particular, the Ariadne-CR and Rathsman-CR models exhibit a large excess of entries at $n^{\rm ch.}_{\rm leading} = 2$ and 4 in Fig. 13a, corresponding to the $Q_{\rm leading} = 0$ bin in Fig. 13b, analogous to the results of Sect. 7.1. From Fig. 13a it is also seen that the Rathsman-CR model predicts a spike at $n^{\rm ch.}_{\rm leading} = 6$. This latter feature was not apparent in the detector level distribution of Fig. 10a because of finite detector resolution.

The corresponding results based on the $y_{\rm min}$ sample are presented in Fig. 14. The data are shown in comparison to the predictions of the Herwig and Herwig-CR models. From Fig. 14a it is seen that the Herwig-CR model predicts a significant excess of events relative to Herwig for $n^{\rm ch.}_{\rm leading} = 2$, 4 and 6, analogous to the results of the Rathsman-CR and Ariadne-CR models

in Fig. 13a. This suggests that the production of events like Fig. 1b is a general feature of color reconnection. The spike in the prediction of the Herwig-CR model at $n^{\rm ch.}_{\rm leading}$=4 in Fig. 14a probably explains the general excess of the Herwig-CR results above Herwig for multiplicities between $n^{\rm ch.}_{\rm leading}$=3 and 5 in Fig. 11.

7.4 Effect of parameter variation on the model predictions

We next study the effect of parameter variation on the predictions of the Rathsman-CR and Ariadne-CR models, to determine if they can be tuned to describe the gluon jet data of Fig. 13 without adversely affecting their descriptions of the inclusive Z^0 decay measurements presented in Sect. 4.

To begin, we define $\Delta Q^{\rm MC-data}_{\rm leading}$ to be the difference between the Monte Carlo prediction and experimental result for the $Q_{\rm leading} = 0$ bin in Fig. 13b. We then vary the principal parameters of the models one at a time, with the other parameters at their standard values, to see if it is possible to reduce $\Delta Q^{\rm MC-data}_{\rm leading}$ to zero or near-zero, i.e. to obtain agreement of the model's prediction with this measurement. We note that if $\Delta Q^{\rm MC-data}_{\rm leading}$ is near-zero, the predictions of the model for the $n^{\rm ch.}_{\rm leading}$ distribution in Fig. 13a will also be in general agreement with the data since the events which yield the excess of entries in Fig. 13b are the same as those which yield the excess in Fig. 13a.

The Rathsman-CR model: For the Rathsman-CR model, the following parameters were varied:

- $\Lambda_{\rm QCD}$, the QCD scale parameter, given by PARJ(81);
- Q_0, the minimum mass value to which partons evolve, given by PARJ(82);
- a and b, which control the longitudinal momentum spectrum of hadrons relative to the string direction in the Lund model of hadronization, given by PARJ(41) and PARJ(42);
- σ_q, which controls the transverse momentum spectrum of hadrons, given by PARJ(21).

The PARJ references are the names of the parameters in the Pythia Monte Carlo. These five parameters are the most important ones controlling the multiplicity and momentum distributions of hadrons in the model. Note we do not include the color reconnection suppression factor R_0 mentioned in Sect. 3 in the above list. It is a trivial result that the Rathsman-CR model will describe the data as well as Jetset for $R_0 \to 0$ since the two models are identical in this limit. Varying R_0 to reproduce the experimental result and corresponding uncertainty for the $Q_{\rm leading} = 0$ bin in Fig. 13b yields $R_0 = 0.0085 \pm 0.0075\,({\rm stat.}) \pm 0.0087\,({\rm syst.})$, consistent with $R_0 = 0$.

The results for $\Delta Q^{\rm MC-data}_{\rm leading}$ are shown in Fig. 15. The standard values of the parameters are indicated by solid dots. The uncertainties attributed to the parameter values in [23], beyond which the description of inclusive Z^0 measurements is significantly degraded if the

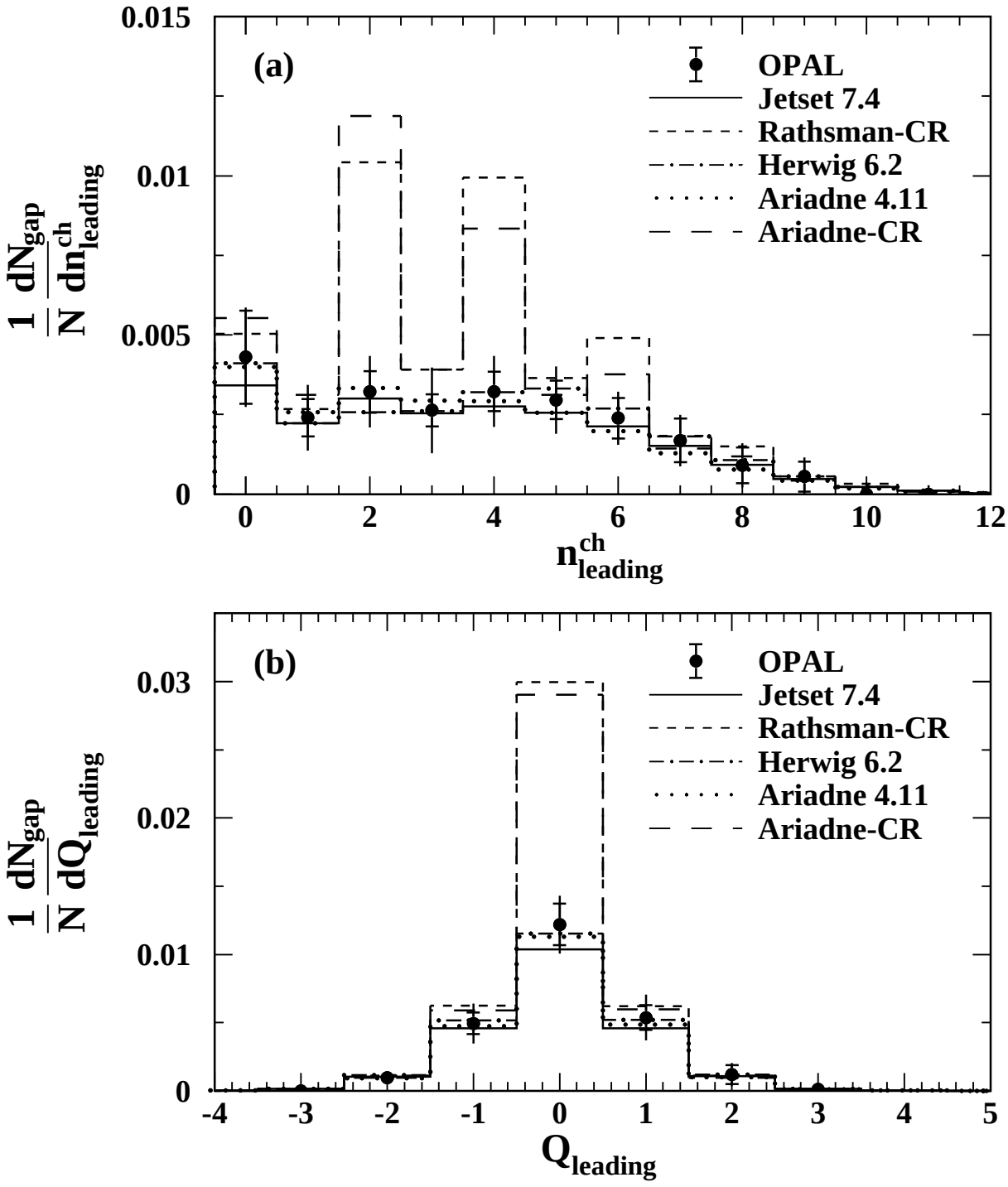

Figure 13: Distributions of (a) $n^{\mathrm{ch.}}_{\mathrm{leading}}$ and (b) Q_{leading} in the leading part of gluon jets, based on our standard selection. "N" represents the total number of selected gluon jets and "$\mathrm{N_{gap}}$" the number of gluon jets with a rapidity gap. The data have been corrected for initial-state photon radiation, gluon jet impurity, and detector response. The horizontal bars indicate the statistical uncertainties. The vertical lines show the total uncertainties, with statistical and systematic terms added in quadrature. The results are shown in comparison to the predictions of QCD Monte Carlo models.

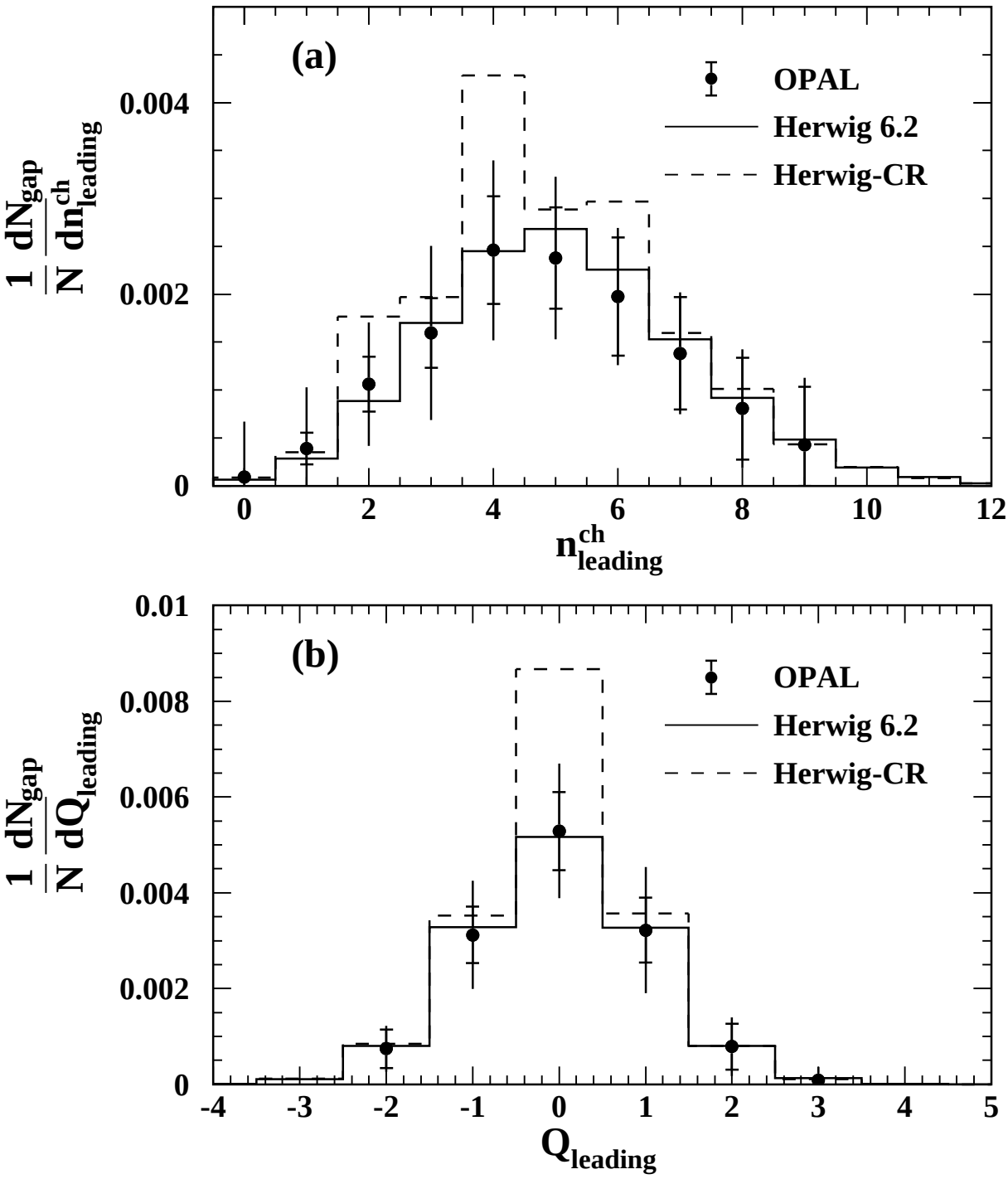

Figure 14: Distributions of (a) $n^{\mathrm{ch.}}_{\mathrm{leading}}$ and (b) Q_{leading} in the leading part of gluon jets, based on the y_{min} selection. "N" represents the total number of selected gluon jets and "$\mathrm{N_{gap}}$" the number of gluon jets with a rapidity gap. The data have been corrected for initial-state photon radiation, gluon jet impurity, and detector response. The horizontal bars indicate the statistical uncertainties. The vertical lines show the total uncertainties, with statistical and systematic terms added in quadrature. The results are shown in comparison to the predictions of the Herwig and Herwig-CR Monte Carlo models.

other parameters remain at their standard values, are indicated by the horizontal error ranges. Note that an uncertainty is not evaluated for the a parameter in [23] and that the uncertainties attributed to $\Lambda_{\rm QCD}$ and b are too small to be visible. The width of the shaded bands in Fig. 15 indicates twice the total experimental uncertainty of $\Delta Q_{\rm leading}^{\rm MC-data}$, corresponding to plus and minus one standard deviation.

It is seen that $\Delta Q_{\rm leading}^{\rm MC-data}$ can be reduced to zero for $\Lambda_{\rm QCD} \approx 1.3$ GeV. As $\Lambda_{\rm QCD}$ is increased, more soft gluons are produced, increasing the probability for multiple color reconnections in an event. In events with multiple reconnections, color strings can reconnect the isolated gluonic string segment illustrated in Fig. 1b back with the rest of the event, spoiling the rapidity gap. From Fig. 15 it is also seen that $\Delta Q_{\rm leading}^{\rm MC-data}$ can be reduced to near-zero for large values of Q_0, e.g. $Q_0 \gtrsim 4$ GeV/c^2. As Q_0 is increased, fewer soft gluons are available, effectively decreasing the reconnection probability. In this sense, an increase in the value of Q_0 is analogous to a reduction in the value of the parameter R_0 discussed above. We note that the values of $\Lambda_{\rm QCD}$ and Q_0 required to reduce $\Delta Q_{\rm leading}^{\rm MC-data}$ to zero or near-zero represent large excursions from their standard values. Fig. 15 suggests it is unlikely that $\Delta Q_{\rm leading}^{\rm MC-data}$ can be reduced to zero or near-zero through variation of a or σ_q.

Setting Q_0 to 3.5 GeV/c^2 with the other parameters at their standard values, the Rathsman-CR model predicts a mean charged multiplicity in inclusive Z^0 events of $\langle n_{\rm ch.}\rangle = 20.2$, smaller than the experimental result of 21.15 ± 0.29 mentioned in Sect. 4. Mean multiplicity in the Lund hadronization model is primarily controlled by the parameters a and b. Therefore, having set $Q_0 = 3.5$ GeV/c^2, we varied the b parameter[7] to reproduce the measured result for $\langle n_{\rm ch.}\rangle$. To increase the prediction for $\langle n_{\rm ch.}\rangle$, b needs to be decreased. As b decreases, $\Delta Q_{\rm leading}^{\rm MC-data}$ also tends to become smaller (see Fig. 15d). By iterating the adjustment of Q_0 and b, it therefore proved possible to simultaneously obtain $\Delta Q_{\rm leading}^{\rm MC-data} \approx 0$ and $\langle n_{\rm ch.}\rangle \approx 21.15$. The result we find for the two parameters is $Q_0 = 5.5$ GeV/c^2 and $b = 0.27$ GeV^{-2}, corresponding to $\Delta Q_{\rm leading}^{\rm MC-data} = 6.7 \times 10^{-7}$. We refer to the Rathsman-CR model with these adjusted parameters as the "re-tuned" Rathsman-CR model.

A one standard deviation limit was evaluated for the re-tuned parameters by adjusting Q_0 and b so they yielded the correct result for $\langle n_{\rm ch.}\rangle$ and agreement with the one standard deviation upper limit for $\Delta Q_{\rm leading}^{\rm MC-data}$ shown in Fig. 15: the result is $Q_0 = 3.7$ GeV/c^2 and $b = 0.35$ GeV^{-2}. A two standard deviation limit was evaluated in an analogous manner, based on twice the total uncertainty of $\Delta Q_{\rm leading}^{\rm MC-data}$: the result is $Q_0 = 3.2$ GeV/c^2 and $b = 0.38$ GeV^{-2}. Finally, Q_0 and b were adjusted to yield $\Delta Q_{\rm leading}^{\rm MC-data} \approx 0$ and a value for $\langle n_{\rm ch.}\rangle$ equal to the LEP-averaged result plus its one standard deviation uncertainty, specifically $\langle n_{\rm ch.}\rangle = 21.44$, see above and Sect. 4. The result is $Q_0 = 5.2$ GeV/c^2 and $b = 0.25$ GeV^{-2}.

We examined the description of the re-tuned Rathsman-CR model for the inclusive Z^0 measurements in Figs. 2–5. The total χ^2 for the 81 bins of data was found to be 1117.7, much larger than the result $\chi^2 = 243.5$ presented in Sect. 4 for the standard version of the Rathsman-CR model (see Table 3). Using the one and two standard deviation limits for the re-tuned parameters, given above, the corresponding χ^2 are 435.1 and 327.2 respectively, still significantly larger than the χ^2 of the standard version. The χ^2 result for the parameters tuned to yield $\langle n_{\rm ch.}\rangle = 21.44$ is 785.2.

[7]The a and b parameters are highly correlated with respect to the model predictions for $\langle n_{\rm ch.}\rangle$; therefore we consider variation of the b parameter alone, not both a and b.

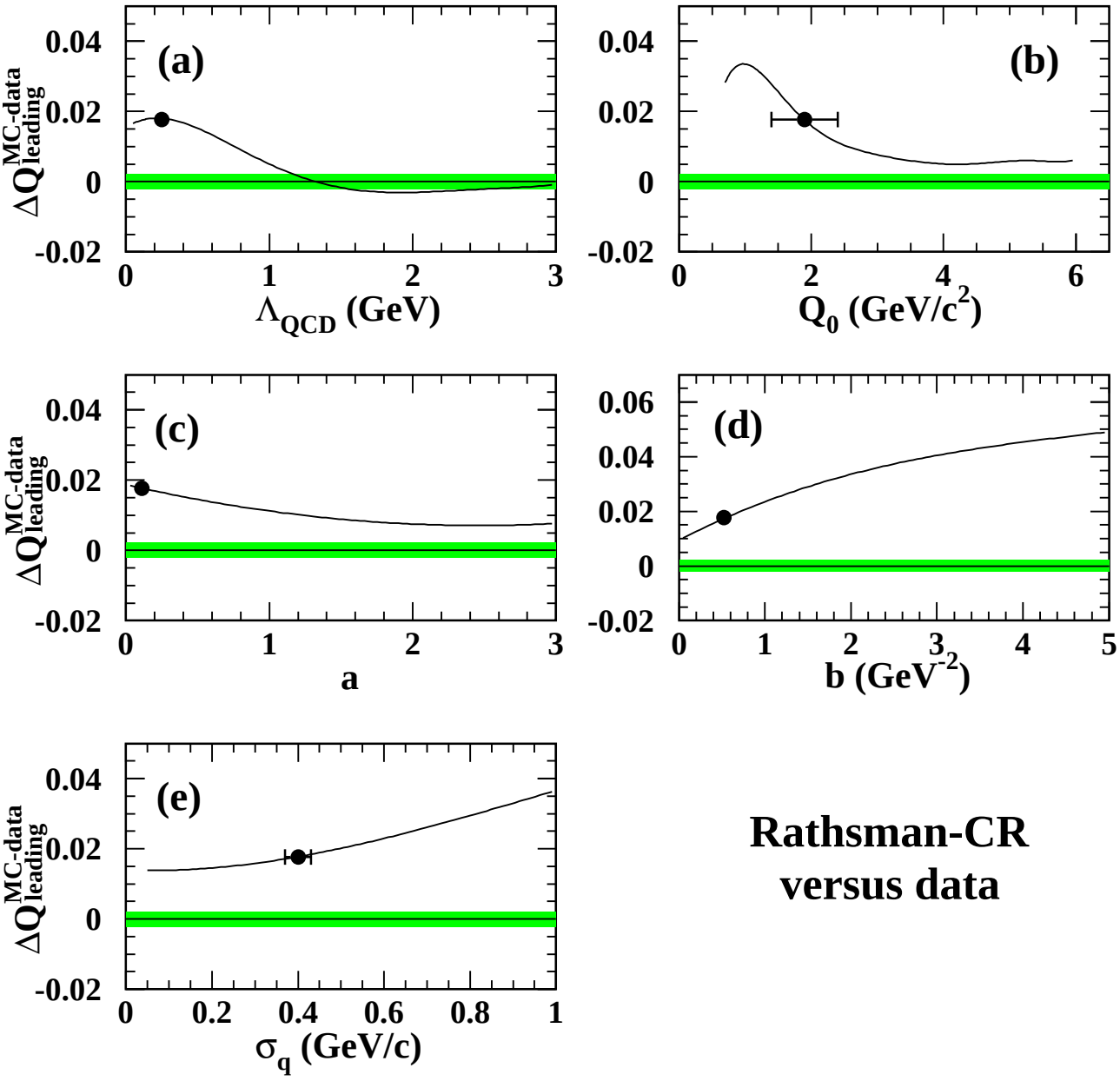

Figure 15: Results for the difference between the Rathsman-CR Monte Carlo prediction and the experimental result for the $Q_{\mathrm{leading}} = 0$ bin in Fig. 13b, $\Delta Q^{\mathrm{MC-data}}_{\mathrm{leading}}$, as the principal parameters of the model are changed with the other parameters at their default settings. The solid dots indicate the standard values of the parameters. The horizontal error ranges show the uncertainties attributed to the parameter values in [23]. For the parameters Λ_{QCD} and b, these uncertainties are too small to be visible. Note an uncertainty is not evaluated for the a parameter. The width of the shaded band centered on $\Delta Q^{\mathrm{MC-data}}_{\mathrm{leading}} = 0$ equals twice the total experimental uncertainty of $\Delta Q^{\mathrm{MC-data}}_{\mathrm{leading}}$.

The χ^2 results for the re-tuned Rathsman-CR model are listed in the bottom portion of Table 3. The deviations of the re-tuned model from the measured distributions are shown by the dotted curves in part (b) of Figs. 2–5.

We attempted to follow an analogous procedure to that described above for Q_0 to adjust $\Lambda_{\rm QCD}$. With $\Lambda_{\rm QCD}$ set to 1.3 GeV and the other parameters at their standard values, the mean charged multiplicity of inclusive Z^0 events is 26.4. To reduce this to 21.15, we increased the value of b. As b increases, $\Delta Q_{\rm leading}^{\rm MC-data}$ becomes larger, however (Fig. 15d), and we could not find a solution which yielded both $\Delta Q_{\rm leading}^{\rm MC-data} \approx 0$ and $\langle n_{\rm ch.} \rangle \approx 21.15$. The closest solution we found, defined by the set of parameters which provided the correct inclusive multiplicity and a minimal result for $\Delta Q_{\rm leading}^{\rm MC-data}$, was $\Lambda_{\rm QCD} = 1.3$ GeV and $b = 4.9$ GeV^{-2}, which yielded $\Delta Q_{\rm leading}^{\rm MC-data} = 0.012$, with $\chi^2 = 2.1 \times 10^4$ for the data of Figs. 2–5.

Last, motivated by the observation that larger values of $\Lambda_{\rm QCD}$ and Q_0 both reduce $\Delta Q_{\rm leading}^{\rm MC-data}$ while having opposite effects on $\langle n_{\rm ch.} \rangle$, we increased both $\Lambda_{\rm QCD}$ and Q_0, with the other parameters at their standard values, to search for a solution with $\Delta Q_{\rm leading}^{\rm MC-data} \approx 0$ and $\langle n_{\rm ch.} \rangle \approx 21.15$. Specifically, we systematically increased the value of $\Lambda_{\rm QCD}$ and then performed a scan to determine the value of Q_0 which yielded the correct result for $\langle n_{\rm ch.} \rangle$. The parameter set with the minimal result for $\Delta Q_{\rm leading}^{\rm MC-data}$ was $\Lambda_{\rm QCD} = 0.6$ GeV and $Q_0 = 4.9$ GeV/c^2, which yielded $\Delta Q_{\rm leading}^{\rm MC-data} = 0.004$, with $\chi^2 = 1606$ for the data of Figs. 2–5.

We conclude it is unlikely that the gluon jet results of Sect. 7.3 can be reproduced by the Rathsman-CR model through variation of $\Lambda_{\rm QCD}$, similar to our observation above for a and σ_q.

Thus, the only mechanism we found to adjust the parameters of the Rathsman-CR model to simultaneously describe our data on rapidity gaps in gluon jets and $\langle n_{\rm ch.} \rangle$ in inclusive Z^0 decays was to increase Q_0 to values in the range from about 3.3 to 5.5 GeV/c^2, much larger than the values of 1–2 GeV/c^2 normally attributed to this parameter. These large values of Q_0 resulted in a significant degradation of the model's description of inclusive Z^0 events, however, as discussed above. We conclude it is unlikely that this model can simultaneously provide a satisfactory description of the data in Sects. 4 and 7.3 using its standard value for the strength of color reconnection, $R_0 = 0.1$. Thus, our results provide compelling evidence to disfavor color reconnection as it is currently implemented by this model.

The Ariadne-CR model: The following parameters of the Ariadne-CR model were varied to determine their influence on $\Delta Q_{\rm leading}^{\rm MC-data}$:

- $\Lambda_{\rm QCD}$, given by PARA(1);
- $p_{T,\rm min.}$, the minimum transverse momentum of a gluon with respect to the dipole which emits it, given by PARA(3);
- a, b and σ_q, given by PARJ(41), PARJ(42) and PARJ(21) as for the Rathsman-CR model.

The PARA references are the names of the parameters in Ariadne, see Table 2. Analogous to our treatment of the Rathsman-CR model, we do not include the color suppression factor PARA(26)

(see Sect. 3) in this list. Varying PARA(26) to reproduce the result for the $Q_{\rm leading}=0$ bin in Fig. 13b, as well as the result for the $Q_{\rm leading}=0$ bin plus its one standard deviation total uncertainty, yields PARA(26) = 96 and 41, respectively, much larger than the standard value PARA(26) = 9. Note that large values of PARA(26) correspond to the limit of large $N_{\rm C}$ in which the probability for color reconnection becomes negligible.

The results are shown in Fig. 16. The standard parameter values are indicated by solid dots. Their uncertainties as given in Table 2 are too small to be visible in the figure. Note an uncertainty was not evaluated for the a or σ_q parameters. Also note the Ariadne computer program requires $\Lambda_{\rm QCD} < p_{T,\rm min.}$. For this reason, the results for $\Lambda_{\rm QCD}$ are shown up to 0.70 GeV only, which is the standard value of $p_{T,\rm min.}$.

The results of Fig. 16 are similar to those of Fig. 15, i.e. $\Delta Q_{\rm leading}^{\rm MC-data}$ approaches zero as the parton shower cutoff $p_{T,\rm min.}$ is increased from its standard value, while it exhibits the same behavior shown in Fig. 15 as a, b and σ_q are varied.

Setting $p_{T,\rm min.} = 2$ GeV/c so that $\Delta Q_{\rm leading}^{\rm MC-data} \approx 0$ (see Fig. 16b), with the other parameters at their standard values, $\langle n_{\rm ch.}\rangle$ in inclusive Z^0 decays is predicted to be 20.0. Through iterative adjustment of $p_{T,\rm min.}$ and b, we found $\Delta Q_{\rm leading}^{\rm MC-data} \approx 0$ (specifically, $\Delta Q_{\rm leading}^{\rm MC-data} = -4.1 \times 10^{-5}$) and $\langle n_{\rm ch.}\rangle \approx 21.15$ for $p_{T,\rm min.} = 4.7$ GeV/c and $b = 0.17$ GeV^{-2}. We refer to the Ariadne-CR model with these adjusted parameters as the "re-tuned" Ariadne-CR model. One and two standard deviation limits were evaluated for the re-tuned parameters in the same manner as described above for the re-tuned Rathsman-CR model; the results are $p_{T,\rm min.} = 2.0$ GeV/c and $b = 0.35$ GeV^{-2}, and $p_{T,\rm min.} = 1.5$ GeV/c and $b = 0.42$ GeV^{-2}, respectively. Similarly, we tuned $p_{T,\rm min.}$ and b to yield $\Delta Q_{\rm leading}^{\rm MC-data} \approx 0$ and $\langle n_{\rm ch.}\rangle = 21.44$, analogous to the procedure in Sect. 7.4: this yielded $p_{T,\rm min.} = 3.5$ GeV/c and $b = 0.20$ GeV^{-2}.

Using the re-tuned parameters to determine the predictions of the model for the data in Figs. 2–5 resulted in a total χ^2 of 3019.3 for those distributions, compared to the result $\chi^2 = 32.4$ presented in Sect. 4 for the standard version of Ariadne-CR (Table 3). For the one and two standard deviation re-tuned parameters, the corresponding results are $\chi^2 = 333.1$ and 132.6, respectively. Thus the description provided by the re-tuned model is much worse than that provided by the standard version, even considering the uncertainties of the re-tuned parameter set. For the parameters tuned to yield $\langle n_{\rm ch.}\rangle = 21.44$, the corresponding χ^2 is 1254.6.

The χ^2 results for the re-tuned Ariadne-CR model are listed in the bottom portion of Table 3. The deviations of the re-tuned model from the measured distributions are shown by the dotted curves in part (c) of Figs. 2-5.

Analogous to the procedure we followed for the Rathsman-CR model, we also attempted to simultaneously describe our gluon jet data and $\langle n_{\rm ch.}\rangle$ in inclusive Z^0 decays by varying both $\Lambda_{\rm QCD}$ and $p_{T,\rm min.}$ with the other parameters at their standard values. The solution which yielded the minimal result for $\Delta Q_{\rm leading}^{\rm MC-data}$ while correctly describing $\langle n_{\rm ch.}\rangle$ was $\Lambda_{\rm QCD} = 0.5$ GeV and $p_{T,\rm min.} = 2.4$ GeV/c, which yielded $\Delta Q_{\rm leading}^{\rm MC-data} = 0.0041$, with $\chi^2 = 2095$ for the data of Figs. 2–5. We did not attempt an adjustment of the two parameters $\Lambda_{\rm QCD}$ and b as we did for the Rathsman-CR model since the value of $\Lambda_{\rm QCD}$ is constrained by $p_{T,\rm min.}$ as explained above.

Thus the only manner we found to adjust the parameters of the Ariadne-CR model to describe our data on gluon jets with a rapidity gap and at the same time yield $\langle n_{\rm ch.}\rangle \approx 21.15$

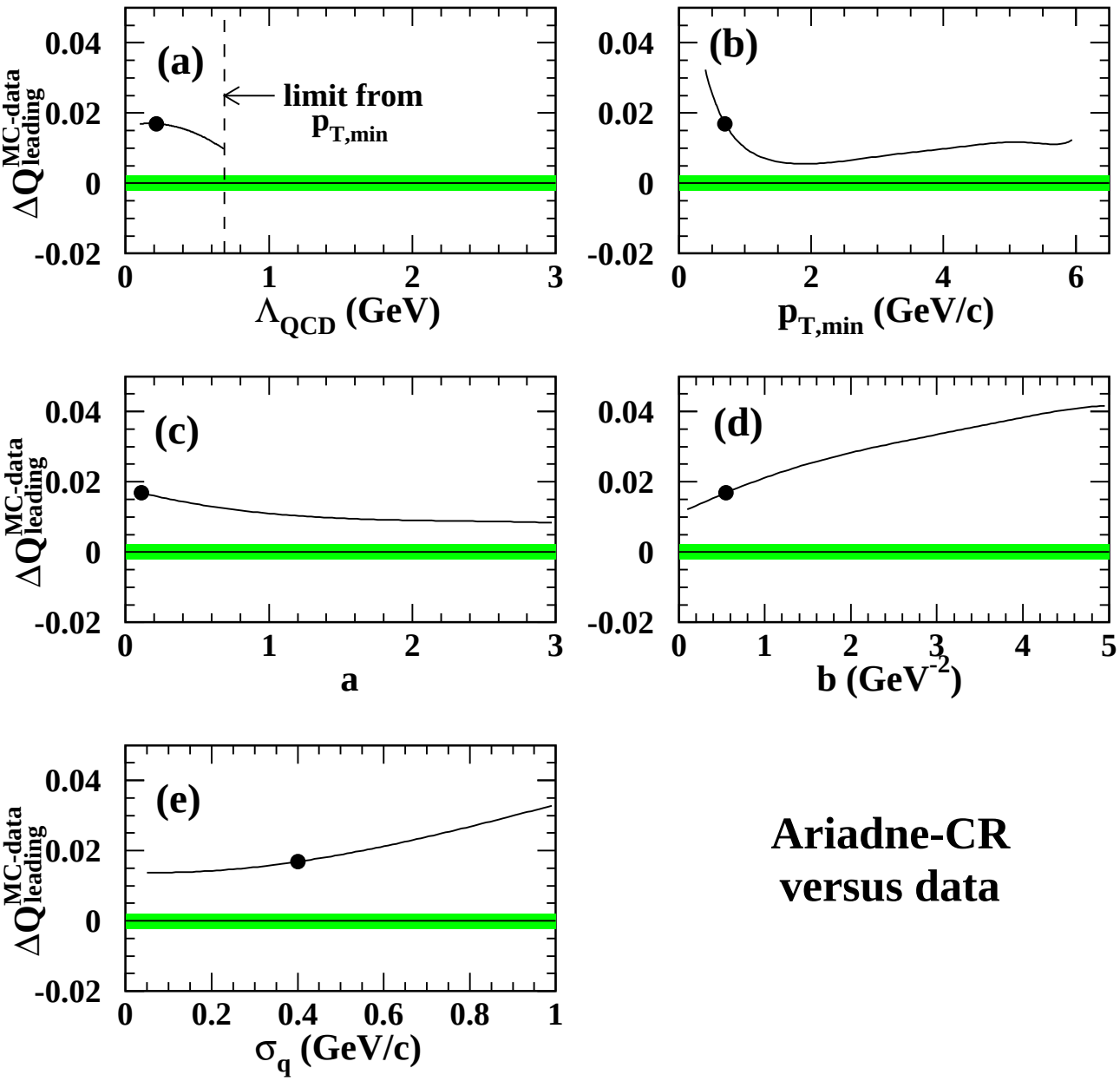

Figure 16: Results for the difference between the Ariadne-CR Monte Carlo prediction and the experimental result for the $Q_{\rm leading} = 0$ bin in Fig. 13b, $\Delta Q^{\rm MC-data}_{\rm leading}$, as the principal parameters of the model are changed with the other parameters at their default settings. The solid dots indicate the standard values of the parameters. The uncertainties attributed to the parameter values in Table 2 are too small to be visible. Note an uncertainty is not evaluated for the a or σ_q parameters. The width of the shaded band centered on $\Delta Q^{\rm MC-data}_{\rm leading} = 0$ equals twice the total experimental uncertainty of $\Delta Q^{\rm MC-data}_{\rm leading}$.

was to increase the parton shower cutoff parameter $p_{T,\mathrm{min.}}$ to values in the range from about 1.6 to 4.7 GeV/c, significantly larger than the range of 0.6–0.7 GeV/c normally attributed to this parameter. This resulted in a significant degradation of the model's description of the global properties of inclusive Z^0 events as described above. Analogous to the Rathsman-CR model, we conclude it is unlikely that the Ariadne-CR model can simultaneously provide a satisfactory description of the data in both Sects. 4 and 7.3 using its standard value for the strength of color reconnection, and that our results provide compelling evidence to disfavor this model.

8 Search for glueball-like resonances

Besides providing a sensitive means to test models of color reconnection, gluon jets with a rapidity gap present an environment which may favor the production of glueballs, as discussed in [9]. If a hard, acollinear gluon in a e^+e^- three-jet $q\overline{q}g$ event propagates a significant distance without radiating, a rapidity gap can form between the gluon jet and the rest of the event. This could enhance the probability for a color octet field to be created between the gluon and residual $q\overline{q}$ system, see Fig. 17a. This octet field is analogous to the field which is expected to connect two separating gluons produced in a color singlet state. This is in contrast to e.g. the Lund hadronization model, in which only color triplet fields are present, see Fig. 17b. Color octet fields provide a natural environment in which to create glueballs [40], through gg pair production from the vacuum, see Fig. 17c.

QCD lattice calculations and other sources (see [41] and references therein) suggest that the mass of the lightest glueball state should lie in the general range from about 1 to 2 GeV/c^2. One of the main candidates for the lightest glueball is the $f_0(1500)$ [42], with a resonance width of 0.11 GeV/c^2. The principal charged particle decay modes of the $f_0(1500)$ are $\pi^+\pi^-$ and $\pi^+\pi^-\pi^+\pi^-$.

Following the suggestions in [9], we therefore examine invariant mass spectra in the leading part of our selected gluon jets. Since we are searching for anomalous resonant structure, the data are compared to the predictions of the models without color reconnection, i.e. Jetset, Ariadne and Herwig. These models do not contain glueballs. The distributions are examined at the detector level only and are normalized to the number of entries in the distributions. The bin widths are adjusted to reflect the mass resolution of the detector, estimated from the simulations.

We begin by examining the total invariant mass of the leading part of the gluon jets, M_{leading}. These masses are determined using both charged and neutral particles. Charged particles are assumed to be pions and neutral particles photons, as stated in Sect. 2. Since glueballs are electrically neutral, we select gluon jets with $Q_{\mathrm{leading}} = 0$, see Fig. 12a. Of the sample of 655 events discussed in Sect. 6, this yields 250 gluon jets. The M_{leading} distribution of these jets is presented in Fig. 18a. The data are shown in comparison to the corresponding results of Jetset, Ariadne and Herwig. The models are seen to describe the data reasonably well. There is a general excess of the data above the Monte Carlo predictions for three bins in the mass range from 1.0 to 2.5 GeV/c^2. The total χ^2 values with respect to the data for these three bins are 11.5 for Jetset, 7.3 for Herwig and 6.0 for Ariadne. Since this excess is only about two standard

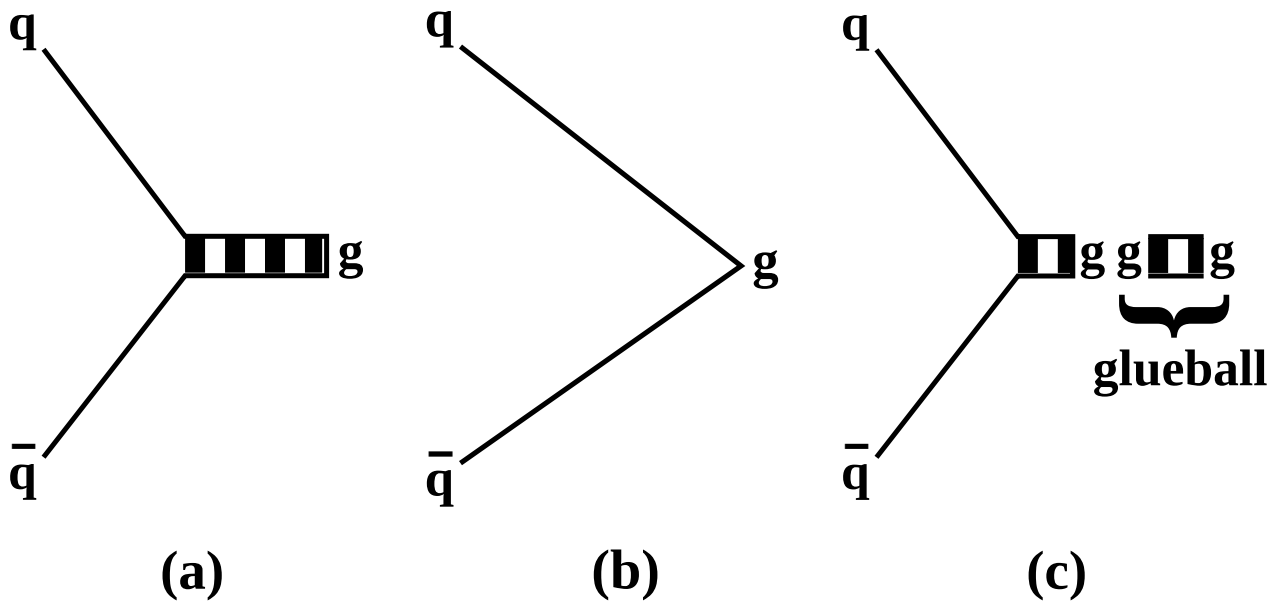

Figure 17: (a) Schematic illustration of a three-jet $q\overline{q}g$ event with a color octet field stretched between the gluon g and residual quark-antiquark $q\overline{q}$ system. The double line with hatching, attached to the gluon, represents the octet field. The single lines connecting the octet field to the quark and antiquark represent color triplet fields. (b) Illustration of a $q\overline{q}g$ event in which color triplet fields connect the gluon directly with the quark and antiquark. (c) The octet field can be neutralized by the production of virtual gg color singlets from the vacuum, leading to the formation of glueballs.

deviations of the statistical uncertainties above the predictions of Herwig and Ariadne[8], it is not possible to obtain a definite conclusion concerning this discrepancy.

Motivated by the charged particle decay modes of the $f_0(1500)$, mentioned above, we also examine the distributions of invariant mass of two oppositely charged particles in the leading part of the gluon jets, $M^{+-}_{\rm leading}$, and the corresponding distribution of four charged particles with total electric charge zero, $M^{+-+-}_{\rm leading}$. The simulations predict that about 75% of the charged particles in the leading part of the selected gluon jets are pions. The distributions of $M^{+-}_{\rm leading}$ and $M^{+-+-}_{\rm leading}$ are presented in Figs. 18b and c. Since in this case the glueball candidate does not necessarily comprise the entire leading part of the gluon jet, there is no reason to constrain $Q_{\rm leading}$ to be zero. Therefore, the $M^{+-}_{\rm leading}$ and $M^{+-+-}_{\rm leading}$ distributions are based on the entire sample of 655 gluon jets with a rapidity gap, not just the jets with $Q_{\rm leading} = 0$. Again, the simulations are seen to describe the data reasonably well. The most significant excess of data above the Monte Carlo predictions occurs in the tail of the $M^{+-+-}_{\rm leading}$ distribution, at mass values between 2.5 and 3.0 GeV/c^2. This excess is about two standard deviations of the statistical uncertainties above the predictions of Ariadne and somewhat larger for the other models. Therefore, we do not observe clear evidence for anomalous resonant structure. Note the spike in the Herwig prediction for $M^{+-}_{\rm leading} \approx 0.77$ GeV/c^2 in Fig. 18b is due to the ρ meson resonance which is too narrow in Herwig. Jetset exhibits a similar effect but at a less significant

[8]The Monte Carlo results are based on about twice as many events as the experimental distributions, see Sects. 2 and 3.

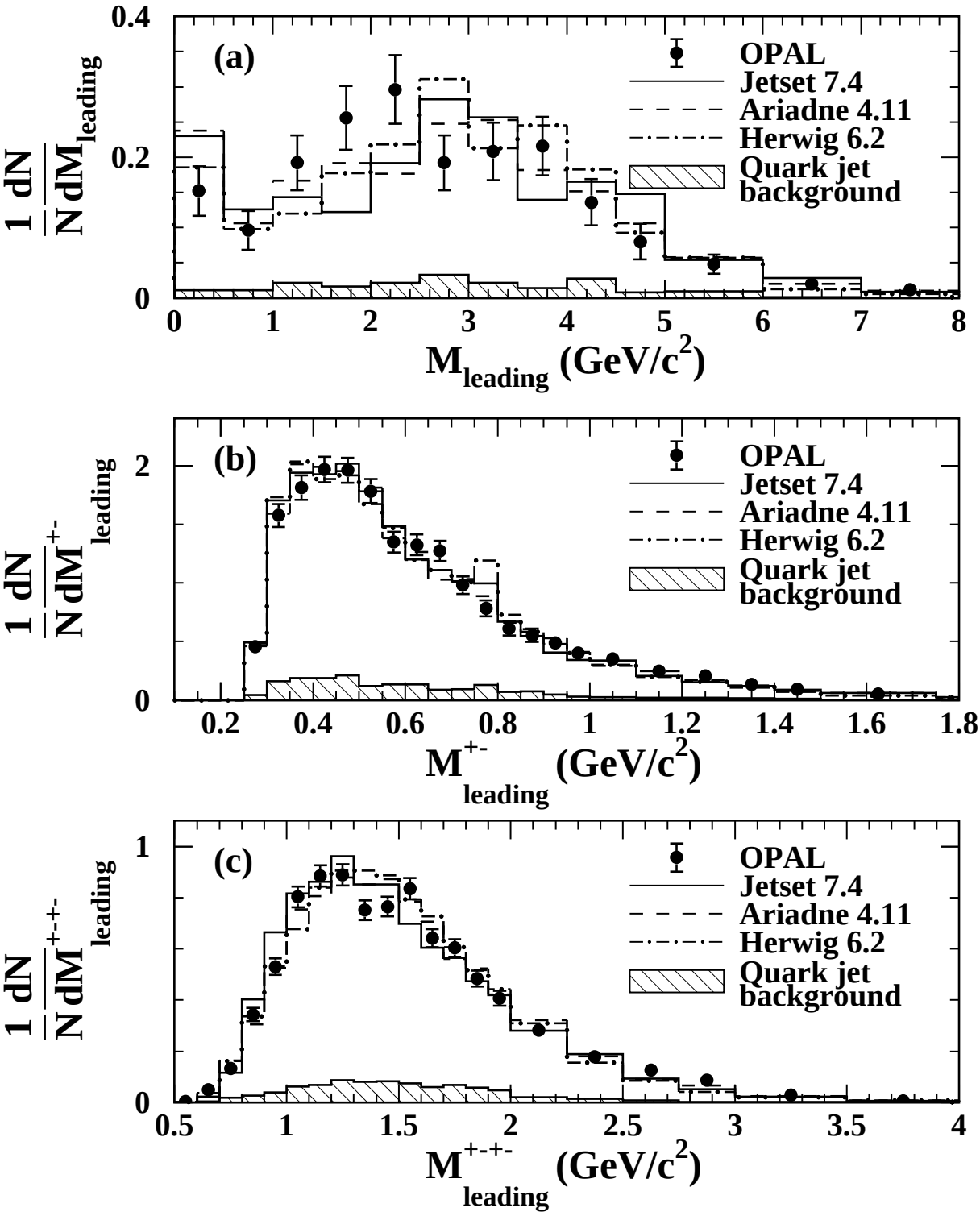

Figure 18: Distribution of jet invariant mass based on charged and neutral particles in the leading part of gluon jets. The distribution includes the effects of initial-state photon radiation and detector acceptance and resolution. The uncertainties are statistical only. The results are shown in comparison to the predictions of QCD Monte Carlo programs which include detector simulation and the same analysis procedures as are applied to the data. The hatched area shows the quark jet background evaluated using Herwig.

level.

To better isolate a signal from a scalar particle such as the $f_0(1500)$, we also examined the $\cos\theta^*$ distribution of charged particle pairs in the leading part of the gluon jets, defined as follows. A "parent" momentum is defined by summing the momenta of two oppositely charged particles. θ^* is the angle between the either of the two "decay" particles and the parent momentum, in the rest frame of the parent. The distribution of $\cos\theta^*$ should be flat for a scalar particle but not necessarily for the combinatoric background. The measured $\cos\theta^*$ distribution was found to be well described by the Monte Carlo simulations. Therefore, we do not obtain any evidence for the anomalous production of scalar particles.

9 Summary and conclusion

A sample of 12 611 gluon jets with a mean energy of 22 GeV and estimated purity of 95% is identified in e^+e^- hadronic Z^0 decay events using b quark jet tagging. The data were collected with the OPAL detector at LEP. A subsample of about 5% of these jets is selected which exhibit a rapidity gap, i.e. an absence of charged and neutral particles over a significant range of rapidity as illustrated in Fig. 7. After imposing the rapidity gap requirement, the estimated purity of the gluon jets is 86%.

We examine the predictions of three models of color reconnection (CR): the Lönnblad model [25] (see also [28]) implemented in the Ariadne Monte Carlo, the Rathsman model [27] implemented in the Pythia Monte Carlo, and the color reconnection model in the Herwig Monte Carlo [18]. We refer to these as the Ariadne-CR, Rathsman-CR, and Herwig-CR models, respectively. Specifically, we examine the predictions of these models for the distributions of charged particle multiplicity and total electric charge in the leading part of the gluon jets, defined by charged and neutral particles beyond the gap.

We find that the Rathsman-CR and Ariadne-CR models predict a large excess of gluon jets with a rapidity gap, for which the leading part of the jets is electrically neutral, compared to the corresponding models without color reconnection. In particular, these two models predict large spikes in the charged particle multiplicity distribution at even values of multiplicity. Thus our analysis is very sensitive to CR effects. We adjust the principal parameters of the two models to determine if they can be tuned to simultaneously provide a good description of our gluon jet measurements and the global properties of inclusive events in hadronic Z^0 decays. We find we can obtain a satisfactory description of the gluon jet data and the mean charged particle multiplicity $\langle n_{\mathrm{ch.}}\rangle$ in inclusive Z^0 events only for very large values of the parton shower cutoff parameters, $Q_0 \approx 3.2$–5.5 GeV/c^2 for the Rathsman-CR model or $p_{T,\mathrm{min.}} \approx 1.5$–$4.7$ GeV/c for the Ariadne-CR model, and that the overall description of global distributions in inclusive Z^0 events is then severely degraded. We conclude that it seems unlikely that either of these two models can be tuned to provide a satisfactory description of both our gluon jet data and the global properties of Z^0 events, using their standard values for the strength of color reconnection. We therefore conclude that color reconnection as currently implemented in these models is disfavored. Our conclusion for the Ariadne-CR model is consistent with our previous results [11]. Here, we present an even more sensitive study of color reconnection and systematically examine the effects of parameter variation on the model's predictions.

The Herwig-CR model also predicts a significant excess of events at even values of charged particle multiplicity in the leading part of gluon jets, compared to the corresponding model without color reconnection, cf. Fig. 14a. These excesses are much less prominent than for the Rathsman-CR and Ariadne-CR models, however, and are not clearly visible once the effects of finite detector resolution are incorporated, cf. Fig. 11. Therefore, we are unable to obtain a definite conclusion concerning this model. The data are nonetheless better described by the version of Herwig without color reconnection.

Our study is also potentially sensitive to the presence of color singlet, electrically neutral objects such as glueballs, see [9]. We therefore examine the total invariant mass distribution of the leading part of gluon jets, using events in which the leading system is electrically neutral. We also examine the invariant mass distributions of two oppositely charged particles, and of four charged particles with total electric charge zero, in the leading part of our sample of gluon jets. We do not observe any evidence for anomalous features in the data, including the production of glueball-like objects.

10 Acknowledgments

We particularly wish to thank the SL Division for the efficient operation of the LEP accelerator at all energies and for their close cooperation with our experimental group. In addition to the support staff at our own institutions we are pleased to acknowledge the

Department of Energy, USA,
National Science Foundation, USA,
Particle Physics and Astronomy Research Council, UK,
Natural Sciences and Engineering Research Council, Canada,
Israel Science Foundation, administered by the Israel Academy of Science and Humanities,
Benoziyo Center for High Energy Physics,
Japanese Ministry of Education, Culture, Sports, Science and Technology (MEXT) and a grant under the MEXT International Science Research Program,
Japanese Society for the Promotion of Science (JSPS),
German Israeli Bi-national Science Foundation (GIF),
Bundesministerium für Bildung und Forschung, Germany,
National Research Council of Canada,
Hungarian Foundation for Scientific Research, OTKA T-038240, and T-042864,
The NWO/NATO Fund for Scientific Research, the Netherlands.

References

[1] S. Brandt et al., Phys. Lett. 12 (1964) 57;
E. Fahri, Phys. Rev. Lett. 39 (1977) 1587.

[2] J.D. Bjorken, Phys. Rev. D47 (1993) 101.

[3] H1 Collab., T. Ahmed et al., Nucl. Phys. B429 (1994) 477;
ZEUS Collab., M. Derrick et al., Phys. Lett. B332 (1994) 228;
ZEUS Collab., M. Derrick et al., Phys. Lett. B369 (1996) 55.

[4] D0 Collab., S. Abachi et al., Phys. Rev. Lett. 72 (1994) 2332;
CDF Collab., F. Abe et al., Phys. Rev. Lett. 74 (1995) 855;
D0 Collab., B. Abbott et al., Phys. Lett. B440 (1998) 189;
CDF Collab., T. Affolder et al., Phys. Rev. Lett. 85 (2000) 4215.

[5] For a recent review, see A.B. Kaidalov, in M. Shifman and B. Ioffe (eds.), *"At the frontier of particle physics,"*, vol. 1, Singapore: World Scientific (2001), p. 603, e-Print Archive: hep-ph/0103011; for a discussion of the pomeron in the context of rapidity gaps, see A. Hebecker, Phys. Rep. 331 (2000) 1.

[6] B. Andersson et al., Phys. Rep. 97 (1983) 31.

[7] G. Gustafson, U. Pettersson and P.M. Zerwas, Phys. Lett. B209 (1988) 90.

[8] OPAL Collab., G. Abbiendi et al., Phys. Lett. B453 (1999) 153;
L3 Collab., M. Acciarri et al., Phys. Lett. B454 (1999) 386;
ALEPH Collab., B. Barate et al., Eur. Phys. J. C17 (2000) 241;
DELPHI Collab., P. Abreu et al., Phys. Lett. B511 (2001) 159.

[9] P. Minkowski and W. Ochs, Phys. Lett. B485 (2000) 139.

[10] SLD Collab., K. Abe et al., Phys. Rev. Lett. 76 (1996) 4886.

[11] OPAL Collab., G. Abbiendi et al., Eur. Phys. J. C11 (1999) 217.

[12] OPAL Collab., K. Ahmet et al., Nucl. Instr. and Meth. A305 (1991) 275.

[13] P.P. Allport et al., Nucl. Instr. and Meth. A346 (1994) 476.

[14] OPAL Collab., G. Alexander et al., Z. Phys. C52 (1991) 175.

[15] OPAL Collab., K. Ackerstaff et al., Eur. Phys. J. C2 (1998) 213;
OPAL Collab., G. Abbiendi et al., Eur. Phys. J. C12 (2000) 567.

[16] T. Sjöstrand, Comp. Phys. Comm. 82 (1994) 74.

[17] G. Marchesini et al., Comp. Phys. Comm. 67 (1992) 465.

[18] G. Corcella et al., JHEP 0101 (2001) 010.

[19] L. Lönnblad, Comp. Phys. Comm. 71 (1992) 15.

[20] See, for example, G. Altarelli, Phys. Rep. 81 (1982) 1.

[21] G.C. Fox and S. Wolfram, Nucl. Phys. B168 (1980) 285.

[22] G. Gustafson, Phys. Lett. B75 (1986) 453;
G. Gustafson and U. Pettersson, Nucl. Phys. B306 (1988) 746;
B. Andersson, G. Gustafson and L. Lönnblad, Nucl. Phys. B339 (1990) 393.

[23] OPAL Collab., G. Alexander et al., Z. Phys. C69 (1996) 543.

[24] ALEPH Collab., R. Barate et al., Phys. Rep. 294 (1998) 1.

[25] L. Lönnblad, Z. Phys. C70 (1996) 107.

[26] L. Lönnblad, private communication.

[27] J. Rathsman, Phys. Lett. B452 (1999) 364.

[28] G. Gustafson and J. Häkkinen, Z. Phys. C64 (1994) 659.

[29] V.A. Khoze and T. Sjöstrand, Z. Phys. C62 (1994) 281; Phys. Rev. Lett. 72 (1994) 28.

[30] See for example R. Enberg, G. Ingelman and N. Timneanu, J. Phys. G26 (2000) 712; Phys. Rev. D64 (2001) 114015.

[31] J. Allison et al., Nucl. Instr. and Meth. A317 (1992) 47.

[32] OPAL Collab., M.Z. Akrawy et al., Z. Phys. C47 (1990) 505.

[33] S. Catani et al., Phys. Lett. B269 (1991) 432.

[34] I.M. Dremin and J.W. Gary, Phys. Rep. 349 (2001) 301.

[35] DELPHI Collab., P. Abreu et al., Phys. Lett. B405 (1997) 202;
ALEPH Collab., R. Barate et al., Phys. Lett. B434 (1998) 437;
OPAL Collab., G. Abbiendi et al., Eur. Phys. J. C18 (2001) 447;
SLD Collab., K. Abe et al, Phys. Lett. B507 (2001) 61.

[36] OPAL Collab., R. Akers et al., Z. Phys. C68 (1995) 179.

[37] Yu.L. Dokshitzer, V.A. Khoze and S.I. Troyan, Sov. J. Nucl. Phys. 47 (1988) 881.

[38] ALEPH Collab., R. Barate et al., Z. Phys. C76 (1997) 191;
DELPHI Collab., P. Abreu et al., Phys. Lett. B449 (1999) 383.

[39] The larger multiplicity of gluon jets relative to quark jets was first observed in OPAL Collab., P.D. Acton et al., Z. Phys. C58 (1993) 387.

[40] C. Peterson and T.F. Walsh, Phys. Lett. B91 (1980) 455.

[41] Particle Data Group, K. Hagiwara et al., Phys. Rev. D66 (2002) 010001.

[42] See, for example, C. Amsler, Phys. Lett. B541 (2002) 22.